Expanding the toolbox for Lanthanide-doped upconversion nanocrystals

IOP Publishing Journal Title
Journal **XX** (XXXX) XXXXXX https://doi.org/XXXX/XXXX

Expanding the Toolbox for Lanthanide-Doped Upconversion Nanocrystals

Yiming Wu[1], Melgious Jin Yan Ang[1,2], Mingzi Sun[3], Bolong Huang[3]* and Xiaogang Liu*[1,2,4]

[1] Department of Chemistry, Faculty of Science, National University of Singapore, Singapore 117543, Singapore
[2] NUS Graduate School for Integrative Sciences and Engineering (NGS), 28 Medical Drive, Singapore 117456, Singapore
[3]Department of Applied Biology and Chemical Technology, The Hong Kong Polytechnic University, Hung Hom, Kowloon, Hong Kong SAR, China
[4]Center for Functional Materials, NUS Research Institute, Suzhou, Jiangsu 215123, China

E-mail: bhuang@polyu.edu.hk
E-mail: chmlx@nus.edu.sg

Received xxxxxx
Accepted for publication xxxxxx
Published xxxxxx

Abstract

The ability to convert low-energy quanta into a quantum of higher energy is critical for a variety of applications, including photovoltaics, volumetric display, bioimaging, multiplexing sensing, super-resolution imaging, optogenetics, and potentially many others. Although the processes of second harmonic generation and multiphoton (or two-photon) absorption can be used to generate photon upconversion, lanthanide-doped upconversion nanocrystals have emerged as an attractive alternative for nonlinear upconversion of near-infrared light with pump intensities several orders of magnitude lower than required by conventional nonlinear crystals. Over the past five years, considerable efforts have been made to tune the photoluminescence of upconversion nanocrystals, and significant progress has been achieved. In this review, we focus on manipulation of the wavelength, emission intensity and lifetime of upconversion nanocrystals. Here, we outline the fundamental principle for the upconversion phenomenon, review the current experimental state-of-the-art for controlling photon upconversion in lanthanide-doped nanocrystals and highlight the prospects for multifunctional upconversion nanocrystals currently in development.

Keywords: lanthanide, upconversion nanoparticle, anti-counterfeiting, security, biodetection, super-resolution imaging, optogenetics, phototherapy, photovoltaics, optoelectronics

1. Introduction

As a nonlinear optical process, photon upconversion can convert near-infrared (NIR) excitation with low photon energy into higher energy ultraviolet and visible luminescence. Since its discovery in bulk crystals in the 1960s, photon upconversion through lanthanide (Ln) ions has garnered tremendous research interest because of its wide-ranging potential applications, spanning from solid-state lasing, IR imaging, security printing, volumetric displays to biological imaging and therapeutics [1-5]. Unlike conventional luminescent systems such as organic dyes and quantum dots, lanthanide-doped upconversion nanoparticles (UCNPs) exhibit excellent photostability, constant light emitting capability, massive anti-stokes shift, sharp multi-peak line emission, and widely tuneable domain of emission lifetime [2]. Such intrinsic features make frequency upconversion by UCNPs appealing for photonic and biological applications. The use of NIR excitation source permits negligible background autofluorescence by eliminating background interference from either endogenous fluorophores or non-specifically bound probes. Moreover, the ability to generate visible optical emission under low dose of NIR irradiation substantially reduces light scattering by

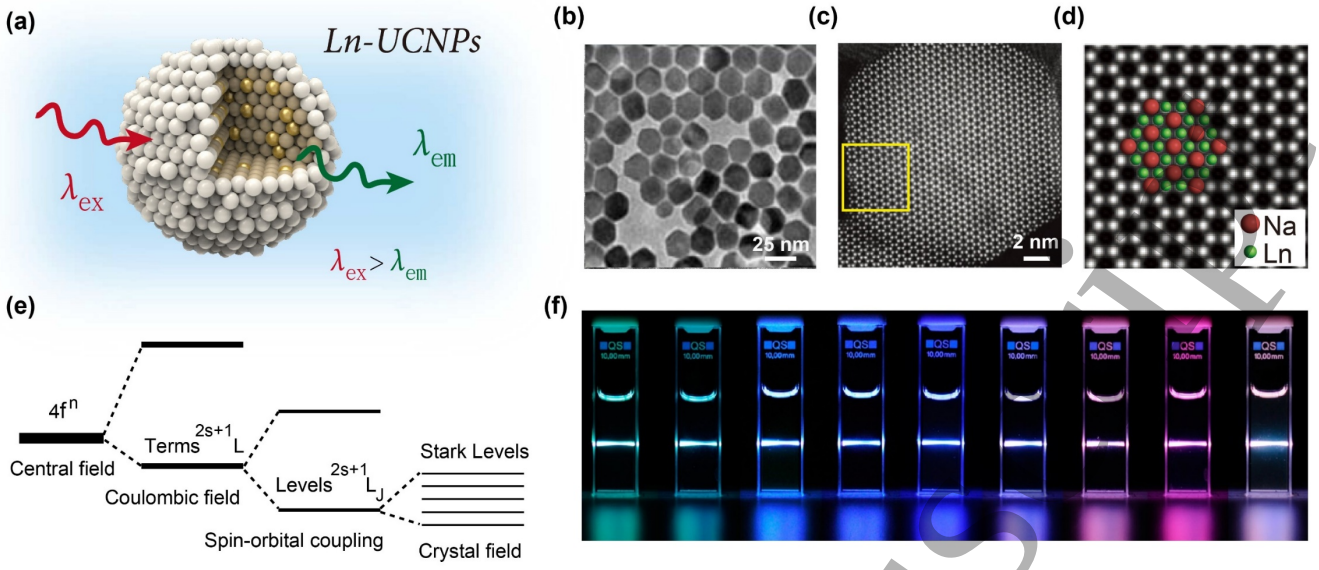

Figure 1. (a) Schematic illustration of upconversion nanoparticle composed of an inorganic crystalline host embedded with trivalent lanthanide dopant ions; (b-c) TEM and High-resolution STEM image of a typical upconversion nanoparticle made of a $NaGdF_4$:Yb/Tm(49/1%) core and a $NaGdF_4$:Tb (15%) shell, revealing the single-crystalline nature of the crystal; (d) An enlarged view of the selected area in c, indicated by a yellow box, showing the lattice imaging of the crystal; (e) Simplified illustration of the effect of Coulombic field, spin–orbital coupling, and crystal field interaction on the electronic configurations of lanthanide atoms; (f) Typical luminescence photographs of colloidal solutions of representative samples showing upconversion multicolor fine-tuning. Figure reproduced with permission from: (b-c), [27], Springer Nature; (f), [33], American Chemical Society.

biological tissues, thereby resulting in less photo-damage to living organisms and allowing deep-tissue phototherapy and imaging to be performed [6]. On the other hand, by converting sub-bandgap NIR photons into usable above-bandgap photons, the use of Ln-doped UCNPs can minimize the non-absorption energy losses in photovoltaic devices, providing a possibility to break the Shockley-Queisser efficiency limit [7-9]. Furthermore, since the excitation wavelength for photon upconversion typically falls in the technologically important telecom window (0.8-1.8μm), UCNPs have become attractive building blocks to be integrated into silicon or other semiconductor materials as spectral converters for the development of telecom wavelength-programmable optoelectronic devices [1,3,10-14].

Over the past decade, substantial research efforts have been devoted to developing high-efficiency UCNPs and exerting control over their optical characteristics. Precise control over the luminescence properties of UCNPs is not only crucial for fundamental mechanistic studies but also extremely important for technology advancement [15-16]. Previous studies have extensively focused on manipulation of the emission properties of UCNPs by conventional chemical routes. These include nanoscale integration, the modification of chemical composition, and core-shell engineering [17-21]. Theoretical calculations from the early work of Crosswhite to the recent development of density functional theory (DFT) have prompted us to investigate the mechanism that controls luminescence properties [22-25]. Recently, innovative strategies through external stimuli have also been proposed to generate tunable upconversion luminescence [26]. Thus far, few attempts have been made to provide a systematic account of various strategies that have been successfully applied to tune the luminescence properties of upconversion nanocrystals as well as to provide a broad overview of their applications in diverse areas. In this review, we begin with a brief description of the fundamental principles of the upconversion phenomenon. Subsequently, we emphasize recent experimental strategies employed to realize on-demand control over the upconversion luminescence in lanthanide-doped nanocrystals, including conventional chemical routes and those beyond chemical methods. The ensuing section highlights some emerging applications involving tunable upconversion luminescence. Finally, several future challenging issues and improvements in this field are discussed in hopes of deepening our understanding of these unique nanosystems.

1.1 Basic considerations

A lanthanide-doped upconversion nanoparticle usually consists of an inorganic and photostable host embedded with various trivalent lanthanide ions (Figure 1a-d) [27]. Unlike conventional anti-Stoke processes, such as second-harmonic generation and multiphoton absorption, photon upconversion in lanthanide-doped nanocrystals relies on the physically existing intermediary energy level, thus possessing higher frequency conversion efficiency. Upconversion emission originates from inner-shell 4*f* electrons which are well-shielded by the complete filled $5s^2$ and $5p^2$ sub-shells of

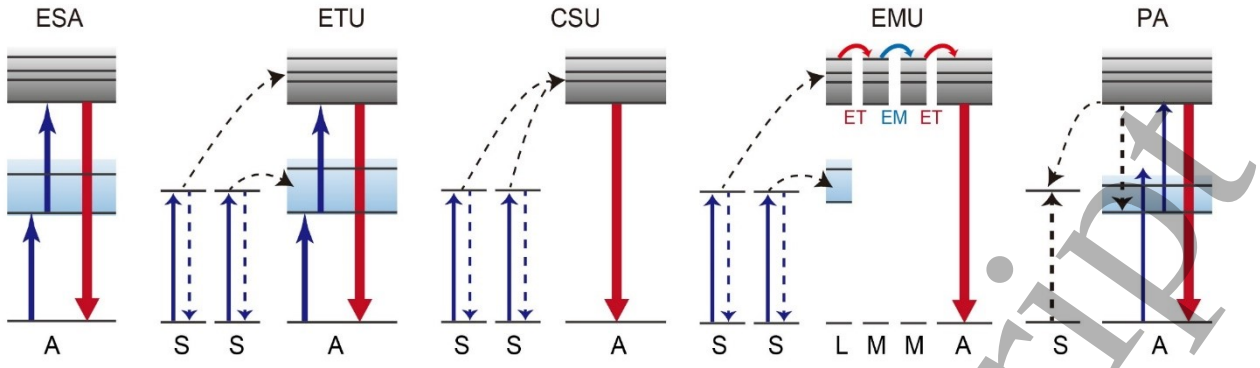

Figure 2. Simplified energy level diagrams depicting upconversion processes including excited-state absorption (ESA), energy transfer upconversion (ETU), cooperative sensitization upconversion (CSU), energy migration upconversion (EMU) and photon avalanche (PA).

lanthanide ions. The optical transitions are localized and generally not affected by quantum confinement. This attribute renders upconversion emissions hardly influenced by the environment, giving rise to unique optical properties such as sharp emission band, reliable photostability and long excited-state lifetime [2].

The repulsion from the Coulombic interaction of the electrons and spin-orbit coupling among *f*-electrons splits the lanthanide's $4f^n$ electronic configuration, inducing a great diversity of energy-level arrangements [28]. This feature makes lanthanides ideal candidates for generating photon upconversion (Figure 1e) [29,30]. Theoretically, lanthanides feature substantially different energy levels and are capable of emitting light at any wavelength due to the diverse distribution of the electrons within 4*f* sub-shells [31,32]. Figure 1f shows a typical luminescence photograph of colloidal solutions of representative Ln-UCNPs featuring the multicolor emission profiles [33]. Many theoretical works published in recent years have been used to explain the electronic structures of rare-earth materials. Based on vibronic coupling, Liu established a semi-empirical model to simulate the experimental spectra [23]. DFT with improved self-consistency calculation method is applied for further understanding and more accurate description of the energy levels of the lanthanide materials [25,28].

1.2 Upconversion luminescence process

Previous fundamental studies on lanthanide-doped crystals have allowed an improved comprehension of the underlying physical phenomenon in photon upconversion processes. With the plentiful ladder-like energy levels of the *4f* electronic configurations, trivalent lanthanide ions can undergo various upconversion processes. Typically, photon upconversion occurs through sequential absorption of two or more low-energy photons and converts the gain to a high-energy state. In principle, upconversion process in Ln-doped UCNPs can be generally categorized into excited state absorption (ESA), energy transfer upconversion (ETU), cooperative sensitization upconversion (CSU), energy migration upconversion (ETU), and photon avalanche (PA) [34-36]. Figure 2 illustrates the proposed upconversion mechanisms, which are described below.

The abovementioned anti-stokes processes are characterized by the conversion of several photons within metastable energy levels of a dopant ion into a long-lived photon state. ESA or ETU are the two common types of upconversion processes relying on the accumulation of the low-energy photons *via* the multiple intermediate states of lanthanide ions. In the ESA process, two low energy photons sequentially absorbed are temporally stabilized in a real intermediary energy level of a single lanthanide ion. For ETU process to proceed, two low-energy photons of the same energy are absorbed by two adjacent sensitizer ions and successively transferred to a neighboring activator ion that can emit from a high energy level through a non-radiative energy transfer process. The major difference between ETU and CSU lies in the absence of a long-lived intermediate energy state of the activator in the latter, and thus the CSU process is much less efficient.

By comparison, upconversion emission arising from the PA process does not depend on the synchronous progress with the ground state within lanthanide ions and could be generated when the power of the excitation exceeds a threshold. On the other hand, four types of lanthanide ions are associated with the EMU process occurring in Gd-based core-shell nanoparticles. A sensitizer first absorbs the excitation photon and then transfers the excited energy to a neighboring accumulator ion. Subsequently, the energy trapped in the accumulator ion is further transferred to a migrator ion to its high-lying excited state. After that, the excited energy can migrate across the core-shell interface through sub-lattice. Finally, the activator harvests the migrating energy to generate upconverted emission. It should be noted that energy transfer upconversion (ETU) is known to be the most efficient frequency upconversion mechanism, which typically occurs in a sensitizer–activator system. After absorbing the excitation photons, resonant energy transfer from the sensitizer to the

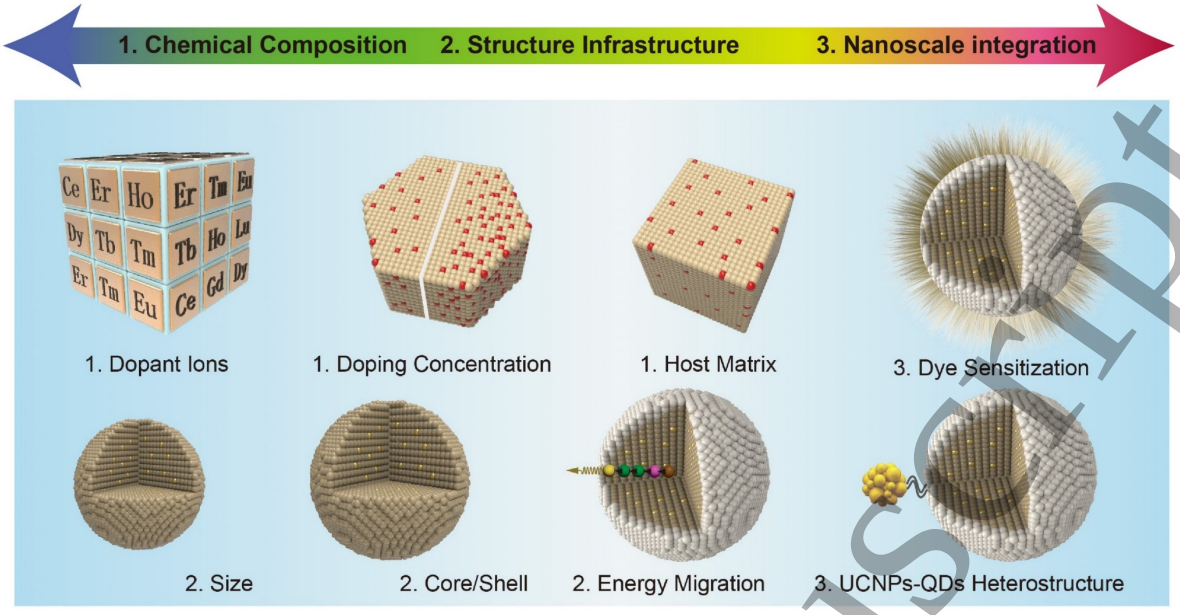

Figure 3. Tuning the luminescence of lanthanide-doped upconversion nanoparticles by conventional chemical methods.

activator populates not only the ground state but also the intermediate state of a nearby activator center. The energy transfer probability W_{S-A} between the sensitizer and activator ions can be described by Förster-Dexter theory:

$$W_{S-A} = \frac{3h^4c^4}{64\pi^5 n^4 \tau_S} \times \frac{Q_{abs}}{R_{S-A}^6} \times \int \frac{f_{em}^S(E) f_{abs}^A(E)}{E^4} dE \quad (1)$$

Where h is the reduced Plank's constant, c is the speed of light in a vacuum, n is the refractive index of the host lattice medium, τ_S is the intrinsic lifetime of the sensitizer ions in the absence of activators, R_{S-A} is the distance between the sensitizer and activator ion, and Q_{abs} is the integrated absorption cross-section of the activator ion. The integral expresses the spectral overlap of sensitizer ion emission and activator ion absorption, as a function of photon energy E ($E = hc/\lambda$). Therefore, one can notice that the R_{S-A} and the spectral overlap are the two critical parameters governing the energy transfer. Besides, high absorbance (Q_{abs}) of the activator at the emission wavelength of the sensitizer and sensitizer ions with lower τ_S is also beneficial for more efficient energy transfer. Moreover, from fundamental ESA process and highly efficient ETU process to EMU process, the use of accurate relative positions of electronic excitations within the host band structures to describe the optical transitions is highly desired. Recently, EMU model has been further improved based on DFT calculations, suggesting the presence of a hidden energy level of Gd ions caused by the close shell effect [37,38]. However, the present challenge for the systematical study of upconversion luminescence is to clarify and quantify the involvement of several mechanisms in one system.

2. The methodology of tuning photon upconversion in lanthanide-doped nanocrystals

Over the past decade, the research on upconversion nanocrystals has made tremendous progress. The ability to precisely modulate the photophysical luminescence properties of upconversion nanocrystals on demand is vital in translating their properties into real-world applications. In this section, we attempt to highlight several key strategies that have been utilized to modulate upconversion luminescence. Broadly, these strategies can be categorized into either "chemical method" or "external stimuli method," as illustrated in Figure 3 and Figure 7. Numerous studies using conventional chemical routes have been reported, including dopant ion variation, host matrix manipulation, spatial confinement of dopants, and nanoscale integration. Alternatively, innovative strategies beyond conventional chemical methods have also been reported to tune the luminescence of upconversion nanocrystals. These include electric or magnetic field-induced tuning, photonic crystal engineering, surface plasmon coupling, microlens light focusing, thermal activation and anisotropic polarization modulation. Theoretical investigations have been proposed in combination with experimental work to exert precise control over upconversion luminescence.

2.1 Tuning through chemical methods

Chemical synthesis routes have been extensively employed to scale up the production of UCNPs with tunable upconversion emissions [13,39-46]. The luminescence of lanthanide-doped nanocrystals primarily originates from the *f-f* transitions of lanthanide ions. Owing to the narrow absorption cross-section of lanthanides, the upconversion quantum efficiencies measured from UCNPs are still far below theoretical values. Therefore, by manipulating the electronic transitions of lanthanide dopants between different energy levels, it is possible to tune the nanoparticle's emission

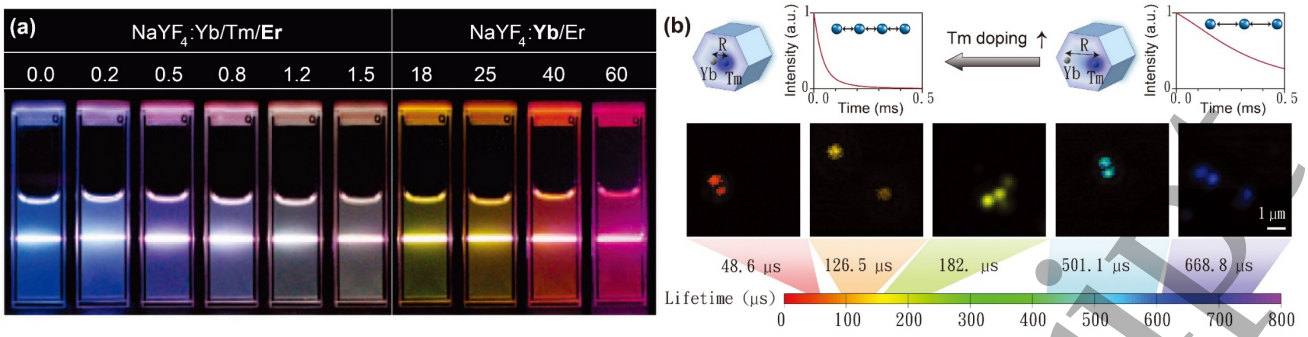

Figure 4. (a) Upconversion multicolor emission photos of $NaYF_4$:Yb^{3+}/Tm^{3+}/Er^{3+} (20/0.2/0.2–1.5 mol%) and $NaYF_4$:Yb^{3+}/Er^{3+} (18–60/2 mol%) nanoparticles in ethanol solutions under 980 nm laser illumination [47]. (b) Schematic illustration of lifetime tuning and time-resolved confocal images for $NaYF_4$:Yb^{3+}/Tm^{3+} (20/0.2-4 mol%) upconversion nanocrystals. The images from left to right represent that nanoparticles with Tm doping concentrations of 4, 2, 1, 0.5 and 0.2 mol%, respectively [53]. Figure reproduced with permission from: (a), [47], American Chemical Society; (b), [53], Springer Nature.

profiles in the form of emission wavelength, intensity, and dynamic decay rate.

2.1.1 Changing the chemical composition and varying dopant concentration

By utilizing different dopant ions, adjusting dopant concentrations and co-doping activators with different emission wavelengths in the host material, multicolor emission of upconversion nanocrystals can be easily achieved. Our group reported the upconversion multicolor fine tuning from red-to-green emission based on $NaYF_4$:Yb^{3+}/Er^{3+} nanoparticles through controlling energy transfer of different lanthanide ions by varying Yb^{3+} concentration [47]. In addition, by carefully co-doping with Er^{3+} and Tm^{3+} in the $NaYF_4$ host material, one could manipulate the emission profiles of UCNPs (Figure 4a). It was found that a subtle change in the Er^{3+} concentration would cause significant changes in emission intensity balance between Er^{3+} and Tm^{3+}, resulting in a wide range of colors from blue to white. Yan and co-workers have systematically studied another co-doped system ($NaYF_4$:Yb^{3+}/Er^{3+}) dependency on the ratio of both dopants, in which they determined the optimal concentration of Yb^{3+} and Er^{3+} to be 20% and 2%, respectively [48]. Besides, several groups have confirmed that such dopant concentration-induced luminescence enhancement is more favorable in higher-order upconversion emission process [49-52].

In principle, the use of the high doping level of luminescent activator ions (Tm^{3+}, Er^{3+}, or Ho^{3+}) permits the maximization of the transfer of the excitation energy absorbed by the Yb^{3+} sensitizers. However, the interaction between different lanthanide activators in the host lattice is usually accompanied by a quenching effect due to deleterious cross-relaxations. In this context, a low dopant concentration is typically implemented to minimize the quenching effect. However, Jin and co-workers reported an intriguing design that utilizes the concentration quenching effect to achieve control over luminescence kinetics [53]. Since the increase in doping concentration would cause an increased rate of energy migration due to reduced ionic distances, a reduction in the emission lifetime of the nanocrystals is expected as a result. By varying the doping concentration of Tm^{3+} activator in the range 0.2–8 mol%, the researchers achieved lifetime modulation with a broad window, ranging from 25.6 μs to 662.4 μs in the blue emission band of Tm^{3+} (Figure 4b). A lifetime-based coding technique through lanthanide doping was also demonstrated, providing a new platform for time-domain optical multiplexing for security applications. Yan and co-workers argued that a high concentration of dopants is likely to induce the clustering effect, particularly within the interplay between Er^{3+} and Yb^{3+}, irrespective of the amount of Er^{3+} sensitizer under study [54].

Tailoring the local crystal field through point symmetry of the luminescent center can loosen the parity-forbidden *4f–4f* intra-configurational transitions of Ln^{3+} ions. The involvement of Li^{+} ions in Ln-doped nanocrystals for upconversion modulation through the symmetry tailoring has been reported by several groups [55-58]. Moreover, Bi^{3+} and Fe^{3+} can also be applied to accomplish the local crystal field tailoring [59,60].

2.1.2 Host matrix screening

The host matrix also plays a critical role in determining the luminescence characteristics of upconversion nanocrystals since the excited energies of the dopant ions may interact with host materials through lattice vibration [21,61-63]. Estimation of quantum efficiency is highly dependent on the energy levels of the host material. Dorenbos has systematically derived the ground levels of Ln^{3+} ions within the bandgap of different host lattices and proved the overlap in the excited states of band structures [64,65]. The precise location of the energy levels of divalent Ln ions relative to the valence and conduction band is proposed based on a three-parameter model as follows:

$$E_{fd}(n, 2+, A) = E_{Afree}(n, 2+) - D(2+, A) \quad (2)$$

$$E_{Vf}(n+1, 2+, A) = E^{CT}(6, 3+, A) + \Delta E_{CT}(n, 6, 3+) \quad (3)$$

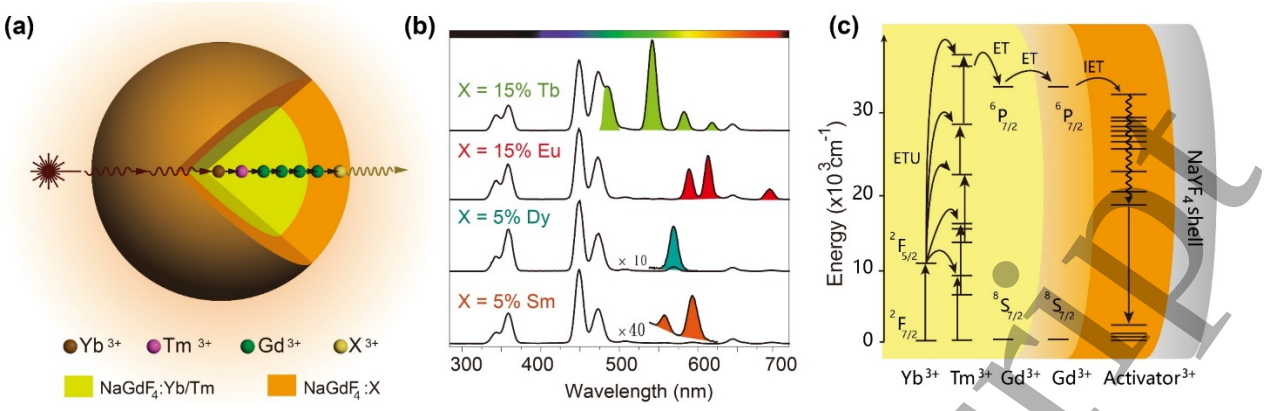

Figure 5. (a) Schematic design of core/shell structured nanoparticles to control upconversion photoluminescence through energy migration-mediated upconversion mechanism. (b) Emission spectra of core/shell structured nanoparticles doped with different activators (Tb^{3+}, Eu^{3+}, Dy^{3+} and Sm^{3+}); (c) Simplified energy level diagrams representing energy migration-mediated upconversion processes; (d) Luminescence photographs of $NaGdF_4$:Yb/Tm@$NaGdF_4$:A@$NaYF_4$ nanoparticles with different activator concentrations in cyclohexane solution under irradiation of a 980 nm laser. Figure reproduced with permission from: (a-b), [27], Springer Nature; (c-d), [33], American Chemical Society.

where $E_{Afree}(n, 2+)$ and $\Delta E_{CT}(n, 6, 3+)$ are constants. $E_{Vf}(n+1, 2+, A)$ is the charge transfer (CT) energy between valence band maximum (VBM) and the 4f ground state of divalent Ln ions and $D(2+, A)$ is the redshift.

The alteration of the host matrix would result in the variation in phonon energy that leads to different upconversion energy transfer pathways. There are numerous observations of structure-dependence of upconverting nanocrystals, especially those with alteration of lattice symmetry [39,43,45,66-68]. A higher enhancement of luminescence emission has been reported for ZrO_2:Er^{3+} in the monoclinic phase than in the tetragonal phase [69]. Even with similar Er energy levels, upconversion intensity in Er-doped Lu_2O_3 is found to be much higher than Er-doped Y_2O_3, which can attribute to a better mixing of 4*f* and 5*d* orbitals in the monoclinic structure rather than other structures [70].

In contrast to oxide materials, fluorides host materials usually have low phonon energies and are commonly used to achieve highly efficient upconversion luminescence. For instance, Zeng *et al.* have been reported the Mn^{2+} and Er^{3+} co-doped $KMnF_3$ nanocrystals [71]. They observed the strong interaction between different lanthanide ions in $KMnF_3$ host nanocrystals, leading to a decrease in the excitation energy at the $^4S_{3/2}$ level of Er^{3+}. This strong interaction subsequently caused an increase in the population at the $^4F_{9/2}$ level of Er^{3+} because of the low phonon energy of the host and the energy transfer from Mn^{2+} to Er^{3+} ions. As a result, this design gives rise to an intensified upconversion luminescence.

2.1.3 Controlling size and utilizing the core-shell architecture

Apart from changing the chemical composition, controlling the size and architecting the core-shell structure of nanocrystals can also achieve tailorable emission [63,72,73]. In the bulk phase of Ln-doped materials, the efficiency of the energy transfer for upconversion luminescence is usually low due to high levels of quenching effects between luminescence centers. The phonons or intrinsic defects in the bulk-sized Ln materials usually facilitate the process of luminescence quenching. As the particle's size decreases, the concentration of surface defects increases [74,75]. Those defects produce near-bandgap trap sites and therefore quench the emission. For example, $NaGdF_4$:Yb^{3+}/Tm^{3+} nanoparticles show a decline in blue emission intensity with decreasing particle size [76]. Similar observations have also been reported in $NaYF_4$:Yb^{3+}/Er^{3+} nanoparticles. Due to the more efficient nonradiative decays across the relevant energy gaps ($^4I_{11/2}\rightarrow$ $^4I_{13/2}$ and $^4S_{3/2}\rightarrow{}^4F_{9/2}$) for smaller particles, the ratio of green-to-red emission and the emission decay time were reduced with decreasing particle size [73]. Theoretical simulations have been used to explain the size-dependent quenching effect of rare-earth materials. For example, DFT calculation method is applied to unravel the potential contribution of the intrinsic defect and doping defects to upconversion emission in CaS [77].

Recently, spatially confinement of dopant ions by utilizing the core-shell architecture as a self-protection strategy has proven useful for mitigating deteriorative quenching effects [27,78,79]. An epitaxial shell layer should suppress or completely block the energy depletion channels from an activator to quenching sites (e.g., defects, impurities, solvent molecules, and capping ligands). This strategy offers a new modality to achieve multicolor upconversion tuning by integrating various dopant ions into a spatially confined nanoscopic region. Multilayer and heterogeneous core-shell structures have also been employed. For example, Wang *et al.* reported the utility of energy migration-mediated process to realize multicolor fine-tuning of upconversion emission (Figure 5) [27]. By coating an inert $NaYF_4$ inert shell on the surface of $NaGdF_4$:Yb^{3+}/Tm^{3+}@$NaGdF_4$:A (A=Tb^{3+}, Eu^{3+}, Dy^{3+}, and Sm^{3+}) nanoparticles, the researchers could drastically boost the emission intensity of the Gd-based nanoparticles [33]. With the assistance of parallel energy

transfer routes, $LiLuF_4$:Yb,Er@$LiLuF_4$ core-shell nanoparticles exhibited a quantum yield of 7.6% [80]. On a separate note, the Yan group recently achieved simultaneous spectral and lifetime tuning based on a five-layer core-shell structure. The researchers introduced noninterfering luminescent regions in the nanosystem to correlate the spectra and lifetime orthogonally with excitation [40].

2.1.4 Surface modifications

Due to the hydrophobic nature of the capping ligands, UCNPs tend to aggregate into clusters in water solution. Many attempts have been documented to alter the wetting property of the UCNPs. A well-established protocol involves the use of a strong acid or an ethanol solution to remove the capping ligands [27,81]. Capobianco and co-workers developed an exciting strategy to enhance the luminescence intensity of UCNPs, based on the protonation of surface-tethered oleate ligands to alter the nanoparticles from hydrophobic to hydrophilic [82]. Alternatively, the upconversion process can be largely boosted by employing organic dyes as broadband sensitizers with large absorption cross-section. For example, in 2012 Zou and co-workers reported that the incorporation of a NIR dye to Yb^{3+} and Er^{3+} co-doped $NaYF_4$ nanoparticles enabled a broadband excitation of the nanoparticles, resulting in a whopping 3,300-fold enhancement in total luminescence intensity [83].

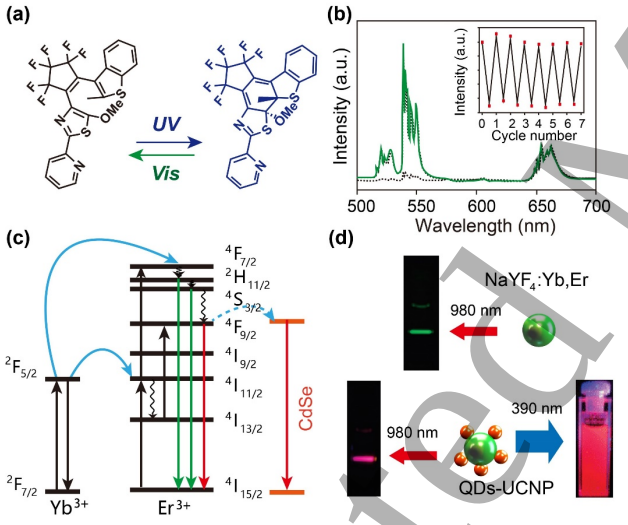

Figure 6. (a) Chemical structures of the diarylethene molecule in the form of open-ring and closed-ring isomers upon photoisomerization. (b) The photoswitching behavior displayed by the composite film made of diarylethene dye-engineered $NaYF_4$:Yb^{3+}/Er^{3+} UCNPs. The inset shows reversible fluorescence on/off cycles under alternating UV/vis irradiation [84]. (c) Schematic of the excitation and energy transfer in CdSe quantum dot-coated $NaYF_4$:Yb^{3+}/Er^{3+} nanocrystals. (d) Photographs of the emission from $NaYF_4$:Yb^{3+}/Er^{3+} nanocrystals (top) and CdSe-coated $NaYF_4$:Yb^{3+}/Er^{3+} nanoheterostructures (bottom) [87]. Figure reproduced with permission from: (a-b), [84], Wiley; (c-d), [87], American Chemical Society.

As an alternative route, the Yan group demonstrated an intriguing strategy to realize a reversible optical tuning by combining photosensitive organic molecules and UCNPs [84]. The change in emission color and intensity of the UCNPs is enabled by rapid energy transfer between dye molecules and the nanoparticles. A reversible transformation of the photochromic molecule occurs between an open-ring isomer and a closed-ring isomer under the alternate irradiation with UV and visible light (Figure 6a). These two isomers exhibit different optical absorption spectra. The change in the optical transmission surrounding the upconversion nanocrystals can reversibly quench the green upconversion emission (Figure 6b). As a result, the upconversion photoluminescence can be modulated by utilizing the reversible absorption character of the photochromic molecules. Polymer encapsulation or coating of inorganic quantum dots can further impart UCNPs with various functional entities for biomedical applications [85,86]. The selective wavelength tuning can also be achieved by placing a different type of optical nanomaterials close to an upconversion nanoparticle. For instance, the emission color tuning from green to pink was reported in a hybrid nanocomposite comprising $NaYF_4$:Yb^{3+}/Er^{3+} nanoparticles and surface-coated CdSe quantum dots (Figure 6c and d) [87].

2.2 Strategies beyond chemical methods

Innovative routes in chemical synthesis have enabled tailored emission profiles by modulating the intrinsic structures of upconversion nanocrystals. In concert with these approaches, the utilization of an external stimulus has recently emerged as an effective method to manipulate upconversion luminescence, which is discussed in the following section (Figure 7).

2.2.1 Diverse excitation sources

For photon upconversion to proceed, Yb^{3+} ion possessing a relatively broad absorption cross-section around 980 nm is usually used as the sensitizer to harvest the excitation energy. However, the 980 nm excitation overlaps with the absorption band of water molecules, which may cause an overheating effect on the tissues after prolonged irradiation or at high power density. One solution that dispenses with overheating is to develop new particle systems, amenable to excitation across a wavelength range with minimal water absorption. For instance, Nd^{3+} ions have been employed to expand the excitation source due to the multiple NIR excitation bands at 730, 808, and 865 nm, respectively [44,88-90]. Zhan and co-workers recently demonstrated that a cost-effective 915 nm laser could be used to replace the conventional 980 nm for deeper tissue imaging with performance comparable to that of 980 nm-based protocols [91].

In addition to NIR excitation, a focused beam of ions can be used to excite lanthanide-doped UCNPs. In 2015, Zhang *et al.* demonstrated that a beam of helium ions (α-beam) could be used as a valid excitation source for pumping upconversion process [92]. The luminescence intensity could be readily tuned by adjusting excitation voltage and current density.

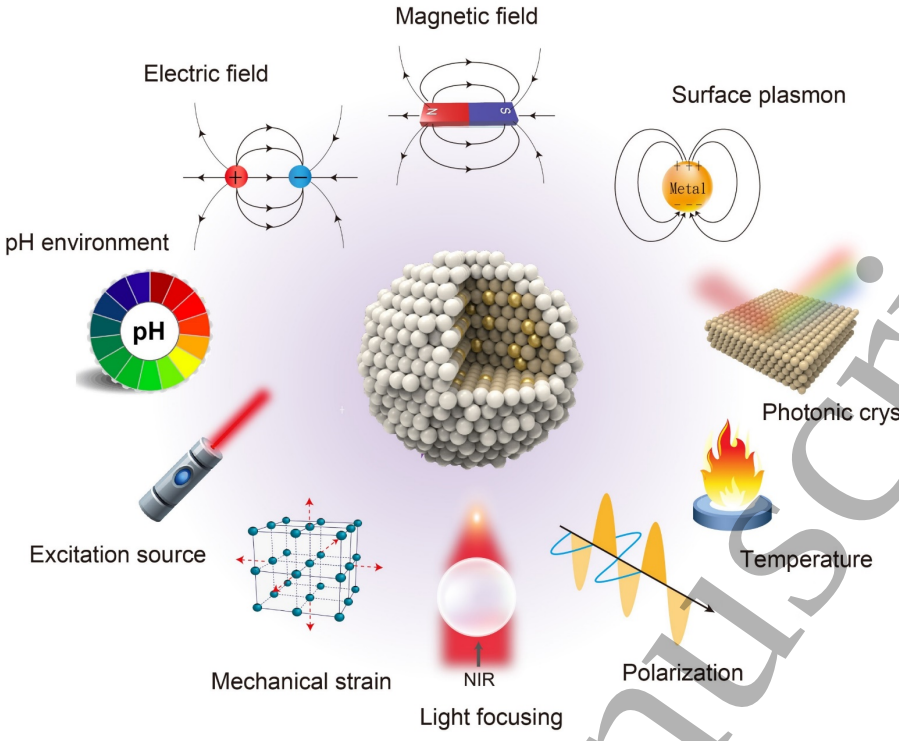

Figure 7. Manipulating the luminescence of lanthanide-doped UCNPs through the control of external stimulus.

Unlike the conventional upconversion processes under NIR laser irradiation, the interaction between the α-beam and the crystal lattice causes the atomic ionization inside the crystal. Subsequently, the ionized secondary electrons can release their energy able to not only excite Yb^{3+} and Tm^{3+} ions but also allow energy transfer from the excited Yb^{3+} to its neighboring Tm^{3+} ions, populating the excited states of Tm^{3+} (Figure 8b). Importantly, this approach enables high-resolution luminescence imaging with a spatial resolution of sub-30 nm (Figure 8b).

Dynamically tunable color emission can also be achieved by the careful manipulation of energy transfer upconversion at the non-steady state. Recently, Deng *et al.* demonstrated a strategy for dynamically fine-tuning the upconversion emission in the full-color range (Figure 8a) [93]. In this design, under the excitation of 808 nm and 980 nm, the upconversion nanocrystals with a multi-shell structure showed different emission colors. For example, when a continuous-wave laser with 808 nm excitation wavelength was used, the emission band appeared mainly at 470 nm, while upon altering the pulse width of the 980nm laser from 200 μs to 6 ms, the emission color was dynamically modulated within the visible range as a result of the changing intensity ratio of the red-to-green emission. These findings provide a new opportunity for precisely controlling upconversion emission in a wide range of applications such as a volumetric display, multiplexed sensing, anti-counterfeiting and so on. In another intriguing demonstration, Zhang and co-workers reported an integrated core-shell-shell nanostructure which can emit a wide range of colors under different excitation power density (Figure 7d) [94]. This feat was realized by the investigation of the transition process within the lanthanide ions. Typically, different activators exhibit different sensitivity to the excitation power density of the laser. In this way, one can control the photon transfer process within the transition pathway and further manipulate the emission colors by varying the excitation laser power density. Notably, the white emission can be generated through the combination of several narrow spectral bands.

Stimulated emission depletion involving the use of a dual-laser system has been adopted to switch on or off the upconversion emission partially. Very recently, Jin and colleagues reported a novel strategy for efficiently suppressing the fluorescent region of the UCNPs to realize super-resolved STED nanoscopy (Figure 8e) [95]. Upconversion nanoparticles with high doping concentration of Tm activator ions ($NaYF_4$: 20% Yb^{3+}/8% Tm^{3+}) were designed and synthesized as the luminescent probe since high doping level of activators often leads to drastically reduced ionic distance and thus strong cross-relaxation between neighboring Tm^{3+} ions, resulting in photon avalanche and population inversion between the $^3H_4$ and $^3H_6$ states. Therefore, the amplified stimulated emission caused by the 808 nm beam can deplete the $_3H^4$ state and switch off the upconversion emission efficiently. Similar observations have been reported in $NaYF_4$:Yb^{3+}/Er^{3+}/$NaYF_4$ core-shell nanoparticles [96]. Under the illumination of 1540 nm infrared laser, the intensity of red emission (655 nm) was reduced due to the emission depletion of the intermediary energy level that interacts resonantly with the depletion beam. Zhan and He also

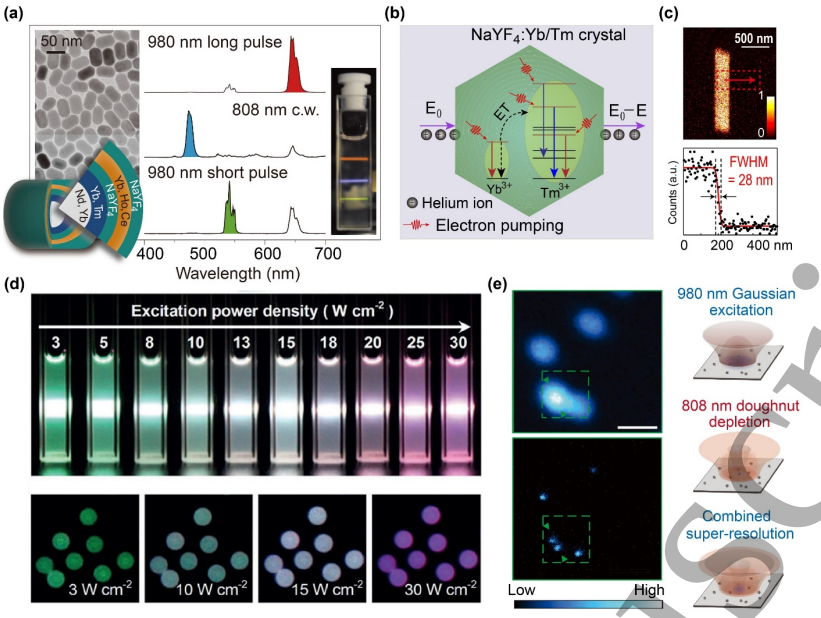

Figure 8. Excitation light-induced multicolor fine-tuning in UCNPs. (a) Core-shell structured $NaYF_4$-based nanocrystals exhibiting three primary color-emitting capability under NIR laser excitation [93]. (b) Proposed upconversion mechanisms of Yb/Tm-codoped system under 980 nm laser and ion-beam stimulation. (c) Iono-luminescence image of a single nanorod and the corresponding line-scanning profile extracted from the intensity counting at the red region along the arrow, indicating an imaging resolution of about 28 nm [92]. (d) Luminescence photographs of $NaYF_4$-coated $NaGdF_4$:Yb/Tm/Er@$NaGdF_4$:Eu nanoparticles in a cyclohexane solution and polystyrene microbeads loaded with the nanocrystals under irradiation of a 980 nm laser with a power density of 3 to 30 W/cm^2 [94]. (e) schematic illustration of $NaYF_4$:Yb^{3+}/Tm^{3+} (20/8%) UCNPs upon 980 nm, 808 nm and dual excitations and the respective confocal and upconversion-STED super-resolution images [95]. Figure reproduced with permission from: (a), [93], Springer Nature; (b-c), [92], Springer Nature; (d), [94], Wiley; (e), [95], Springer Nature.

proposed similar work on achieving super-resolution of bio-image based on $NaYF_4$:18% Yb^{3+}, 10% Tm^{3+} nanoparticles with even higher Tm doping concentration. They applied a single pair of excitation/depletion beam (810 nm) and acquired 96% depletion of blue emission (455 nm). Therefore, by switching on/off depletion beam, the upconversion emission could be modulated, which can significantly lower the intensity requirements of laser depletion [97].

2.2.2 Theoretical investigation

Due to the unique electronic structure of the lanthanide elements, the dynamics of their upconversion luminescence properties has become more complicated because of the variation in both chemical and electronic structures. Theoretical understanding of basic electronic structures, spectral properties, and energy levels is of great importance to guide the tuning process for upconversion luminescence. Since 1960, the electronic structure of lanthanide materials has been well documented in the pioneering works of Judd *et al.* [50-52,54,55]. These works provided a theoretical foundation that subsequently benefited the work of Crosswhite and Carnall, who proposed and applied the empirical operator model in Ln-doped solids [22,98]. Carnall and co-workers systematically analyzed a series of Ln-doped LaF_3 materials with different optical transitions within the $4f^n$ configuration. By combining energy matrices and free-ion terms with a crystal field, they successfully correlated the transition energy with theoretical energy levels. Hence, these basic models allowed the calculation of the free ion energy levels and splitting in $4f^n$ orbitals [99].

In principle, Laporte's parity selection rule implies that electric dipole intra-*4f* transitions are forbidden, while *4f-5d* transitions are allowed. The phonon-electron interactions induced by lanthanide doping can modify the optical property of lanthanide emitters and somewhat relax the selection rule. The vibronic transition also contributes significantly to the broadband absorption and emission in Ln-doped materials. Hence, it is necessary to investigate vibronic transition and phonon-assisted energy transfer in order to control upconversion dynamics.

Chen and Liu interpreted the spectrum of Er-doped Y_2O_2S material at a low temperature in terms of the confinement effects based on a study of phonon density of states (PDOS) [100]. They estimated the population ratio of Er^{3+} on two ground levels as follows:

$$\frac{N1}{N2} \approx \frac{W_{LIT} + W_{Raman,abs} + W_{21,abs}}{W_{Raman} + W_{21}} = e^{-\frac{\Delta E_{21}}{kT}} + \frac{W_{LIT}}{W_{Raman} + W_{21}} \quad (4)$$

where W_{LIT} is the rate of laser-induced thermalization through nonradiative relaxation on the excited states (populating), $W_{Raman,\ abs,}$ and W_{Raman} are the rates of two Raman phonon absorption and emission, respectively. W_{21} is the spontaneous

phonon emission from ground level 2 to level 1. All these competition processes lead to an equilibrium population at the $^4I_{15/2}$ upper ground state. The nanocrystal size effect on PDOS and the phono-relaxation rates was calculated. The numerous hot bands in the spectrum from the $^4I_{15/2}$ ground state to $^4F_{7/2}$ excited state can be attributed to the lack of low-energy phonon modes, which leads to a reduction in energy transfer efficiency. Later, Liu has established a semi-empirical model to simulate the experimental spectra based on vibronic modes [23]. Based on constrained frequency degeneracy modes as Eq. (5) and vibronic coupling strength with specific line width, the luminescence spectra of the $Y_3Al_5O_{12}$ material can be constructed from modeling with detailed analyzation of energy levels, vibronic modes, and coupling constants.

$$\mathrm{I(E)} = \sum_k C_k(\Delta E_k) f_{m,n}(E, \omega_1, \omega_{2,k}) \quad (5)$$

The rapid development of computational resources makes DFT calculations a powerful method to improve our understanding of the energy transfer mechanism underlying the upconversion process [38,61,101,102]. For example, Yan and Huang investigated the electronic structures of the β-phase alkali-earth fluorides and analyzed the origins of the different observation on the fundamental band structures [37]. The understanding of EMU model has been improved with more accurate Gd *4f* levels based on the different overlap of F-Ln orbitals. The narrower bandgap of $NaGdF_4$ originated from a shifting 4f-empty state toward the bandgap. Within the first Brillouin zone, the local disorder can modulate the valence band near the Γ point.

Recently, the Huang group proposed a new route of energy transfer based on clustering effect from high dopant concentrations [54]. An Er-Yb-Er self-sensitized upconversion mechanism has been proposed to enhance the UC energy transfer based on the unusual absorption behaviors is determined by the Yb^{3+} dopants instead of sensitizers. Converse to the conventional idea, the researchers utilize a conventional quench pathway to create an in-shell to in-core route assisted by the interface region. The interlayers showed apparent potential difference arises from the band-offset effect that would de-excite the electrons from higher Yb_Y^{3+} levels to a lower Er_Y^{3+} level and reach red upconversion emission. Therefore, more details can be supplied from the different theoretical works that benefit our understanding of the upconversion energy transfer mechanism and create more possibilities in manipulating the upconversion luminescence in future experiments.

2.2.3 Surface plasmon coupling

Beyond traditional surface modification, surface plasmon technique has great potential in optoelectronic controlling, which based on the coherent oscillation coupling of free electrons with the excitation light [103-106]. Commonly, plasmons in noble metal nanoparticles with size much smaller than the incident wavelength (< 20 nm) are called localized surface plasmon resonance (LSPR), which can be adjusted by controlling their morphology, chemical composition, and spatial configuration. The plasmon damping dynamics is mainly dominated by three processes including electron-hole generation, thermalization, and photon emission. In particular, for a metal with a size close to the quantum region, the electron-electron interaction becomes essential. When approaching the nanosize regime, the corresponding electric field distribution of nanoparticles will be altered. Based on the approximation of quasistatic theories, the distortion of electron cloud induced by the altered electron field can be expressed by the metal polarizability with the scattering, absorption, and extinction cross-sections of a noble metal as follows [107]:

$$\alpha(\lambda) = V_{NP} \frac{\varepsilon(\lambda) - \varepsilon_m(\lambda)}{3\varepsilon_m(\lambda) + 3L_i(\varepsilon(\lambda) - \varepsilon_m(\lambda))} \quad (6)$$

$$\mathrm{C_{abs,i}} = kIm(\propto(\lambda)) \quad (7)$$

$$\mathrm{C_{scat,i}} = \frac{k^4}{6\pi}|\propto(\lambda)|^4 \quad (8)$$

where λ represents the light wavelength, V_{NP} is the volume of nanoparticles, k is the wave vector, and L_i is the depolarization factor that varies with the metal morphology. ε and ε_m are the dielectric constant of metal and the non-absorbing surrounding material, respectively. Because of this local field effect, the excitation field as well as the emission decay rate can be enhanced, but also quenching by energy back-transfer from emission center to metal structures is possible. Thus, this local field effect shows potentials for manipulating upconversion emission in terms of emission intensity, wavelength, and decay rate [108-111].

In different situations, the plasmonic resonance structure can extend the upconversion emission at various levels when the plasmonic resonance coincides with the absorption band or emission band of UC luminescence. For instance, with noble metal NPs nearby, the absorption cross-section of the UCNPs can be expressed as [112]:

$$\sigma_{abs} \propto \omega Im[\alpha](\frac{E_{loc}}{E_0})^2 \cos^2\theta \quad (9)$$

Moreover, the expression of quantum yield (Q) will also be affected with contribution from the LSPR induced by Au NPs as follows [113,114]:

$$\mathrm{Q} = \frac{\Gamma_{Rad} + \Gamma_{Rad}^M}{\Gamma_{Rad} + \Gamma_{Rad}^M + \Gamma_{NRad} + \Gamma_{NRad}^M} \quad (10)$$

Where Γ_{Rad} and Γ_{NRad} represents the radiative rates and non-radiative rates, respectively. The Γ_{Rad}^M term is the contribution from plasmon resonance influence, which can increase the emission rate by the local electromagnetic field enhancement. For high quantum yield fluorescence materials, the influence from Γ_{Rad}^M is limited. However, for low quantum yield fluorescence materials, the Γ_{Rad}^M can enhance the value of Q evidently.

Gold nanoparticles are the best candidate for coupling with UCNPs since the surface plasmon band of Au nanoparticles is tunable from the visible-to-NIR range in favor of the light harvesting by UCNPs. The leading causes of the LSPR modulation on upconversion luminescence include the amplification of the local electromagnetic field and the

enhancement of recombination rate. In 2009, first work about applying LSPR in enhancing upconversion luminescence intensity had been reported by the Yan group based on the coupling of Ag nanowires with $NaYF_4$:Yb,Er nanocrystals [115]. Both green and red emission intensity has been improved with an increase factor of 2.3 and 3.7, respectively.

Recently, there are some research works focused on the coupling structure on the single particle level to tune upconversion emission properties and investigate the mechanism in detail [116-118]. The LSPR properties are mainly determined by the nanostructure and local environment, in which different geometry of the noble metals have shown distinct effects. For example, Hartschuh and colleagues reported a system comprised a good nanotip with $NaYF_4$:Yb^{3+}/Er^{3+} nanoparticles, demonstrating how the locally enhanced electric fields in the vicinity of a sharp metal tip can amplify the excitation and emission rates of a nearby upconversion nanoparticle, as shown in Figure 9a [119]. In this case, when a gold nanotip was placed close to a single $NaYF_4$:Yb^{3+}/Er^{3+} nanoparticle, both the green emission and red emission was enhanced as can be seen in the tip up/down spectra in Figure 9b and 9c. Besides, Au or Ag arrays and grating films [120], Au nanohole array [121], gold pyramid array [122], Au nanocavity array [123] are also investigated by different groups for improving the upconversion emissions.

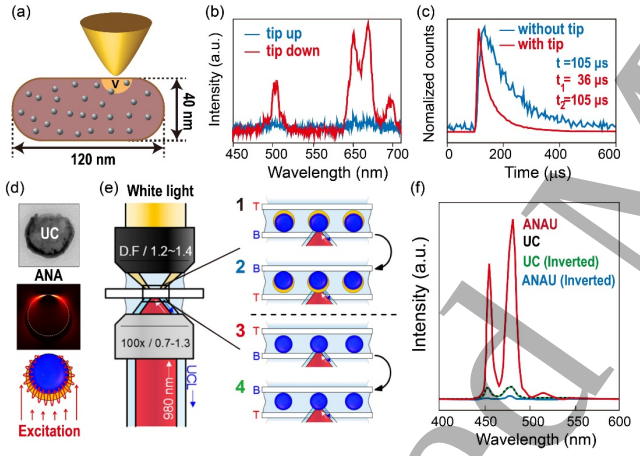

Figure 9. (a) Schematic illustration of tip-enhanced photoluminescence in $NaYF_4$:Yb^{3+}/Er^{3+} UCNPs. (b,c) Corresponding upconversion emission spectra and lifetime measurements near the gold nanotip (blue) and away from gold nanotip [119]. (d) TEM image and schematic diagram of ANAUs depicting nanofocusing of the excitation light of ANAUs with nanocrescent antenna. (e) Schematic diagram of experimental setup used to measure the asymmetric emission characteristics of various samples. The sample was vertically mounted (1 and 3) to measure the emission toward the nanocrescent antenna tip region, while for the measurement of emission toward the body region, the sample was mounted in an inverted direction (2 and 4). (f) Emission spectra of an ANAU toward the tip region (black), an ANAU toward the body region (blue), a UC toward the bottom (red), and a UC toward the top (green) [126]. Figure reproduced with permission from: (a-c), [119], American Chemical Society; (d-f), [126], American Chemical Society.

In core-shell structures, the spatial parameter is another important effect for LSPR properties. Optimization on the distance between noble metals and UCNPs have been carried out by many research groups as well [124,125]. These results suggested that upconversion emission profiles can be modulated by varying the distance between the nanoparticle and the plasmonic center.

In another separate work, Lee and co-works developed a novel hybrid structure with an asymmetric nanocrescent antenna on upconversion nanoparticle (ANAU). This plasmonic antenna can deliver excitation light effectively to the upconversion nanoparticle by nanofocusing light, giving rise to asymmetric frequency upconverted emission concentrated toward the tip region [126]. The single upconversion nanoparticle was confined in the asymmetric nanocrescent antenna and exhibited directionality-dependent frequency upconverted emission (Figure 9d and e). In this system, a 16.1 times enhancement of photon emission toward the nanocrescent antenna tip region were generated by ANAU, whereas photon emission is reduced by half toward the nanocrescent antenna body (Figure 9f).

2.2.4 Magnetic and electric field-induced tuning

Compared to the conventional chemical tuning strategies, dynamically adjusting energy level splitting or crystal lattice initiating the energy pathways are alternative routes that allow for dynamic and in-situ modulation of upconversion luminescence. For example, the Hao group reported an electric field induced modulation of upconversion emission [127]. By applying a bias voltage to the ferroelectric host material $BaTiO_3$ with Yb^{3+} and Er^{3+}, dynamically luminescence tuning and enhanced upconversion emission were observed through the converse piezoelectric effect (Figure 10). The enhancement and modulation of upconversion photoluminescence can be attributed to the increased variation of Er^{3+} site symmetry because of the distinct structure symmetry of the $BaTiO_3$ host affected by an electric field.

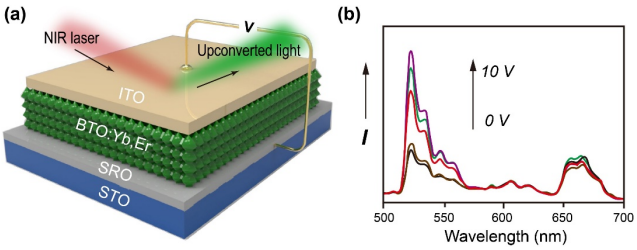

Figure 10. (a) Schematic illustration of opto-electrical device based on Yb^{3+} and Er^{3+} co-doped ferroelectric host material ($BaTiO_3$). The active matrix was sandwiched between two transparent conductive electrodes. (b) Upconversion photoluminescence can be modulated by adjusting the applied bias voltage to the ferroelectric $BaTiO_3$ thin film. Figure reproduced with permission from [127], Wiley.

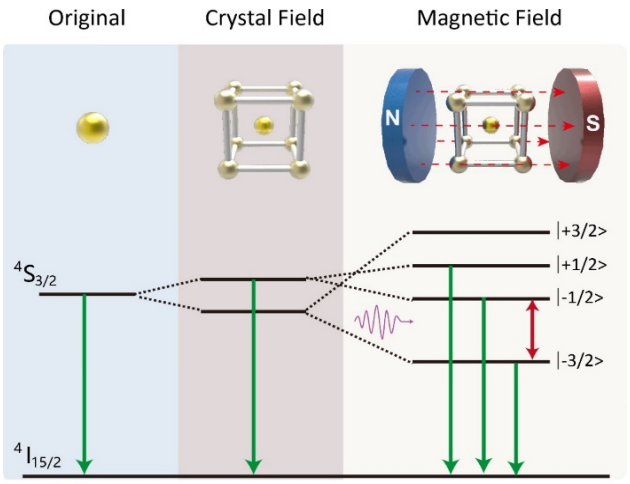

Figure 11. General schematic diagram for the splitting energy levels of $_4S^{3/2}$ of the Er^{3+} ions in which the gap between the Zeeman levels |-1/2> and |-3/2> increases with applied magnetic field. Figure reproduced with permission from [129], Wiley.

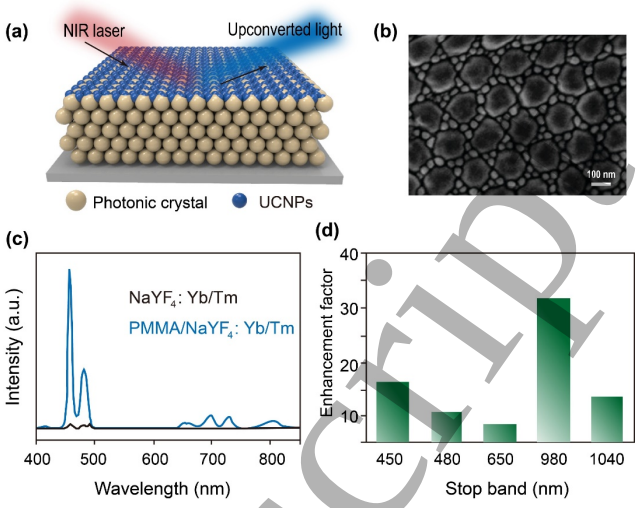

Figure 12. (a) Schematic illustration of photonic crystals deposited with a layer of UCNPs. (b) SEM image of the as-prepared PMMA photonic crystal with $NaYF_4$:Yb^{3+}/Tm^{3+} nanoparticles deposited on the photonic crystal substrate. (c) Upconversion emission spectra of $NaYF_4$:Yb^{3+}/Tm^{3+} nanoparticles recorded with and without the PMMA photonic crystal. (d) Different emission enhancement factors obtained using PMMA photonic crystals with different photonic stop bands. Figure reproduced with permission from [137], The Royal Society of Chemistry.

The large bandgap and local non-crystallization of surface structures of UCNPs can largely influence their upconversion emission. A better understanding and utilization on the energy levels can assist in modulating the upconversion optical properties. The Meijerink group has observed the effect of the electric dipole and magnetic dipole on the emitters [128]. Different dependence index in cavity model of Eu-doped and Gd-doped $NaYF_4$ has been measured and calculated to describe the radiative transition probability between different energy levels. Further modulation on upconversion emission can be expected based on theoretical and experimental results. The Li group developed a similar strategy to tune upconversion luminescence by introducing a magnetic field. The external magnetic field was used to manipulate the energy level of the doped lanthanide ions to control upconversion luminescence [129]. The magnetic tuning mechanism of the green emission is due to the Zeeman splitting of $^4S_{3/2}$ energy levels of the Er^{3+} ions. A general schematic diagram for energy levels splitting of Er^{3+} ions is explained in Figure 11, especially the $^4S_{3/2}$ and $^4I_{15/2}$ energy states are often available for the stabilization of the excited ions. Induced by an applied magnetic field, $^4S_{3/2}$ of Er^{3+} cracks to four different energy levels: |+3/2>, |-3/2>, |+1/2>, |-1/2>. When the external magnetic field gets stronger, the distance between |-3/2> and |-1/2> is increased, resulting in that |3/2> doublet state is further splitting. Meanwhile, the chance for the slight radiative transition from |+3/2> to |3/2> will be increased since most upconversion luminescence comes from the lowest |-3/2> state of Er^{3+} ions. Consequently, the upconversion emission in the visible range could be reduced. Similar observations have been reported in a recent work [130].

2.2.5 Photonic crystal engineering

Photonic crystals have been widely used to manipulate the emission intensity and lifetime of the upconverters within the structure [131-136]. Periodic dielectric structure-based three-dimensional photonic crystals permit the manipulation of the flow of light to generate photonic bandgaps. By making an optimal factor, the photonic crystals can provide high electric field intensity within the structure. Thus, the interaction between the upconversion emitter and its local electromagnetic state affects the spontaneous and stimulated emission process, resulting in enhanced emission without quenching effects. Recently, several groups achieved the sizable enhancements of upconversion emission by depositing UCNPs on the surface layer of photonic crystals. Different modulating effects were observed, depending upon the position of emitters within the 3D structure, the type of the photonic crystal and the refractive index of the building blocks. For instance, the Song group investigated the coupling effect of UCNPs on a photonic crystal made of polymethyl methacrylate (PMMA) opals [137]. The researchers fabricated periodic structures by depositing $NaYF_4$:Yb^{3+}/Tm^{3+} nanoparticles on the surface of the photonic crystal (Figure 12). They achieved more than 30-fold emission enhancement when the excitation frequency matched with the stop band of the photonic crystal. It was found that the stop band of the PMMA photonic crystal actively contributed to the level of upconversion enhancement.

2.2.6 Altering the pH environment

The pH scale can have an effect on the state of upconversion photoluminescence. The pH value is a general

parameter which is determined by the concentration of hydrogen ions in solution. The hydrogen ions may affect the interaction among the emitter ions directly or change the upconversion emission indirectly by modifying the parameters in control of the upconversion process. For example, the Capobianco group observed that upconversion luminescence could be regulated by tuning the pH environment of ligand-free $NaYF_4$:Yb^{3+}/Er^{3+} nanoparticles through acid treatment. This phenomenon may attribute to different multiphonon relaxation processes among several excited states of the emitter ions when surface-bound OH groups have been affected by the pH change [82].

In another study, the Hao group showed a hybrid system composed of silica-coated $NaYF_4$: Yb^{3+}/Er^{3+} nanoparticles and cysteine–Au NPs. The pH value can control the assembly process of AuNPs and further modulate the upconversion emission [138]. In this way, upconversion luminescence may be switched depending on the changes of OH ions concentration in the reaction system. For mechanism, the cysteine linking the AuNPs is pH sensitive so the reversible assembly of AuNPs can be controlled by destroying and rebuilding the linkage. Moreover, the plasmon absorption band of these AuNPs matches with the emission band of UCNPs, and by changing the size and morphology of AuNPs, the absorption bands can be red-shifted to some extent. As a result, upon tuning the pH value, the green and red upconversion photoluminescence are finally affected. Wolfbeis and his co-workers also observed such a phenomenon in the $NaYF_4$: Yb^{3+}/Er^{3+} nanorod system, which can be applied to a biomedical pH sensor [139].

2.2.7 Microlens light focusing

Microlens has been widely used for increasing the light concentration efficiency of solar cells or light extraction efficiency of LED [140-144]. The light field confinement by the micro-lens provides an exciting possibility for fluorescence enhancement. Recently, Li and co-works reported that spherical or discal shape bio-cells, such as yeast cell and human cell are able to focus light into a confined region, which can act as a biological microlens to enhance the fluorescence of UCNPs (Figure 13) [145]. It was found that the NIR excitation light was confined in a subwavelength region due to the photonic nanojet effect of the bio-micro-lens, resulting in a 100-fold enhancement of upconversion luminescence. They further experimentally demonstrated single-cell imaging and real-time detection of pathogenic bacteria, which is difficult to achieve by using conventional methods, mainly due to the small sizes of pathogenic bacteria and high motilities in dark environments.

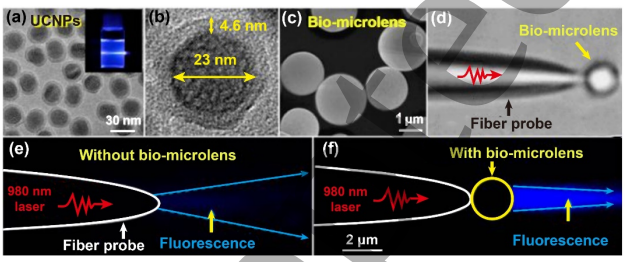

Figure 13. (a,b) TEM image of the core-shell UCNPs with an overall diameter of 28 ± 3 nm. (c) SEM image of the yeast cell bio-microlenses with an average diameter of 2.0 μm. (d) Optical image showing a bio-microlens was trapped at the tip of an optical fiber probe. (e,f) Fluorescent images of output light from a fiber probe, recorded by 980 nm laser excitation without or with a bio-microlens. Figure reproduced with permission from [145], American Chemical Society.

2.2.8 Thermal phonon activation

A phonon represents an excited state of vibrations of elastic structures of materials, playing a significant role in governing electrical and thermal conductivities of a material. Previous reports showed that the process of upconversion luminescence involves various non-radiative transitions whose non-radiative transition rates usually depend on the environmental temperature [146-148]. Therefore, since the gaps among energy levels of lanthanide ions can be changed at different temperatures, the upconversion emission is subject to tuning according to a distinct temperature. For example, Li and colleagues investigated the temperature-related upconversion emission properties of Yb^{3+}, Er^{3+} co-doped $NaYF_4$ UCNPs with different particle phases and sizes [149]. They discovered that the intensity of upconversion emission within β-phase UCNPs showed the largest value at about 100 K, while that of α-phase UCNPs exhibited emission quenching problem when the temperature was increased.

In another case, Jin and co-workers reported an unprecedented enhancement of upconversion emission from small-sized UCNPs with increasing temperature [150]. They proposed that the vibrations of surface-bound molecules through Yb–O chelating can work as surface phonons to broaden the excited-state energy band of the Yb^{3+} sensitizer and reduce the energy mismatch between the sensitizer and activator, as illustrated in Figure 14a. This principle facilitates the energy transfer from Yb^{3+} to adjacent activators and permits the luminescence of an upconversion process to be significantly intensified (Figure 14b). It was found that this anomalous upconversion emission enhancement effect related to the changing of temperature is depending on the size of UCNPs when the temperature is high, and this relationship becomes weak when the size of UCNPs gets larger. This thermally enhanced upconversion phenomena due to surface phonon-assisted energy transfer process of UCNPs with the relatively smaller size indicated that the surface phonon engineering could be used to overtake the thermal quenching effect of small-sized UCNPs.

Thermal activation combined with upconversion is found to be useful in enhancing solar energy efficiency by altering the inadequate response to low solar energy photon. Yan and Wang have unraveled a novel route for altering the unabsorbed low-energy photons into a high-energy one, which can reach a 16% power upconversion efficiency in Yb^{3+} doped

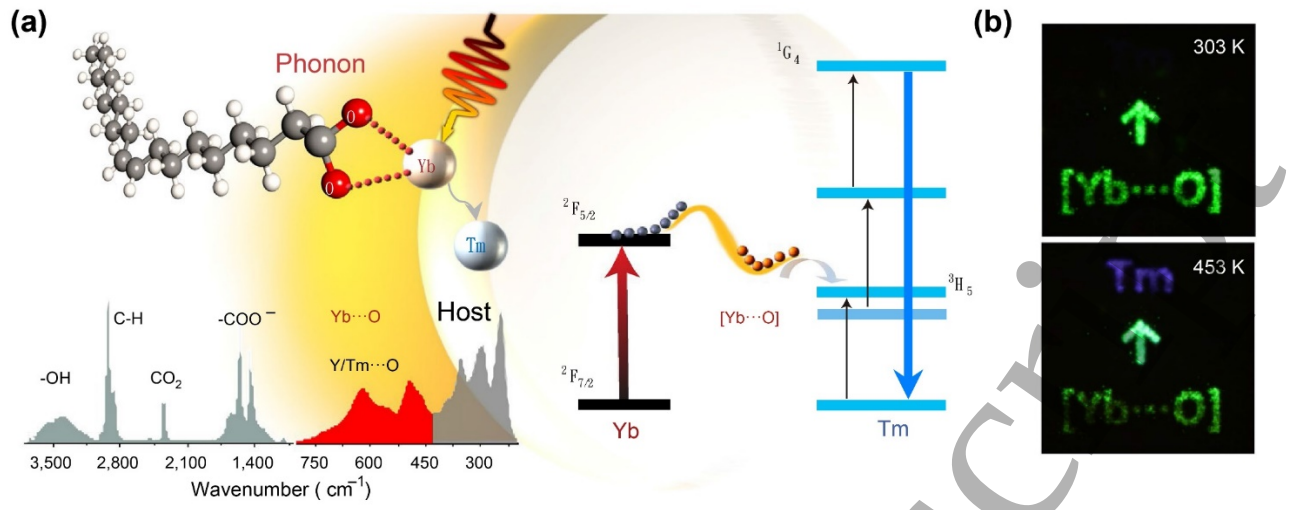

Figure 14. (a) Schematic illustration of the surface-phonon-enhanced upconversion process; (b) Temperature-responsive anti-counterfeiting security patterns at 453 K and 303 K. Figure reproduced with permission from [150], Springer Nature.

ZrO_2 [151]. They also supplied guidelines for finding proper host matrix to achieve higher upconversion emission including high melting points, low thermal conductivities and strong absorption to infrared light.

2.2.9 Mechanical stress-induced tuning

Upconversion luminescence mainly originates from the parity-forbidden *f-f* electron transition of lanthanide ions. Relaxing this selection rule where electric dipole transitions are weakly allowed could lead to an increased probability of the electric dipole transitions and improved upconversion quantum efficiency [18,152]. Therefore, tailored emission properties can be achieved by carefully engineering the surrounding crystal field environments of the lanthanide ions. For instance, Dionne and co-workers found a strain-induced enhancement in upconversion emission in the $NaYF_4$ system by altering the geometry of the $NaYF_4$ host matrix. By manipulating the local symmetry to relax the Laporte selection rule and distances between Ln ions to increase the electron transitions probability, a 2-fold enhancement in upconversion emission from α-$NaYF_4$:Yb^{3+}/Er^{3+} nanoparticles was observed, as shown in Figure 15 [153].

Alternatively, since the transition metals with *d–d* transitions are susceptible to the surrounding environment, doping transition metals inside UCNPs is expected to be a promising approach to tune the upconversion emission. Recently, the same research team led by Dionne reported a mechanical force-induced tuning of upconversion luminescence from an Mn^{2+},Yb^{3+},Er^{3+} co-doped $NaYF_4$ system [154]. In this system, Mn^{2+} ion was used to substitute Y^{3+} ion in the lattice partially, and it further served as a pressure sensor to the lanthanide pair. After that, an alternative energy pathway was created when Mn^{2+} was involved in the Er^{3+}-dominated energy transfer, leading to the conversion of photons from the green to the red state of Er^{3+}. Consequently, an external force will lead to changes in the external crystal field of Mn^{2+}, as accompanied by a color change due to the variation in the relative intensity of green to red emission.

Many materials that can exhibit both mechanoluminescence (ML) and upconversion luminescence are potential candidates for applications in monitoring pressure and temperature distribution. Piezoelectric semiconductor CaZnOS with high stability and a wide bandgap is considered to be an excellent multifunctional host matrix to introduce rare-earth doping and realize upconversion luminescence. The Pan group reported that the intensity of the green emission in Er-doped CaZnOS is proportional to applied pressure [155]. Moreover, the doped sample also shows bright visible emission upon 980 nm excitation. They utilized the high sensitivity of the fluorescence intensity ratio of $^2H_{11/2}$ and $^4S_{3/2} \rightarrow {}^4I_{15/2}$ of Er^{3+} in the upconversion process for temperature sensing. In the same host system, Peng and his

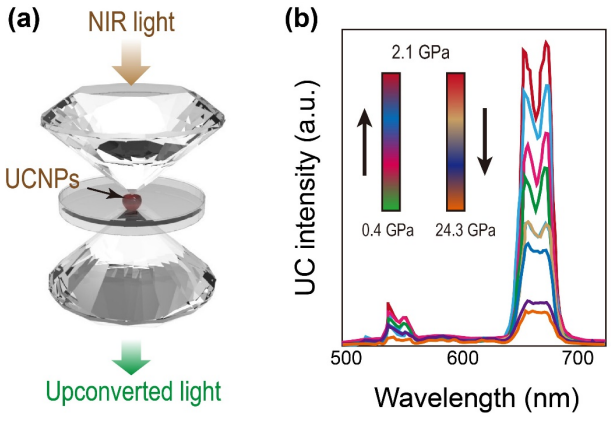

Figure 15. (a) Illustration of the experimental approach used in pressure-dependent spectra measurement. (b) Pressure-dependent emission spectra of α-$NaYF_4$:Yb^{3+}/Er^{3+} UCNPs on 980 nm excitation. Figure reproduced with permission from [153], American Chemical Society.

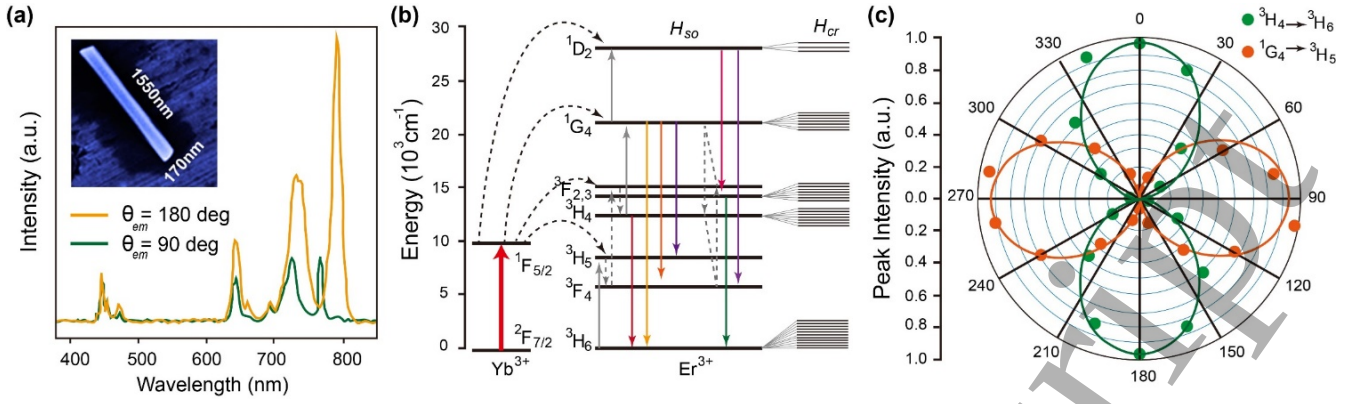

Figure 16. (a) Upconversion emission spectra of a single $NaYF_4:Yb^{3+}/Tm^{3+}$ rod, recorded at different polarization angles. Inset is the scanning electron microscopic image of the single rod. (b) Proposed energy transfer pathways from Yb^{3+} to Tm^{3+}, alongside schematic splitting levels of Tm^{3+} because of crystal field interaction. (c) Polar plots of the upconversion peak intensity (according to the $_3H^4 \rightarrow {}_3H^6$ and $_1G^4 \rightarrow {}_3H^5$ transitions of Tm^{3+}) as a function of the emission polarization angle. Figure reproduced with permission from [159], American Chemical Society.

co-workers also discovered the external force-induced upconversion luminescence in the NIR region spanning the first and second tissue-penetrating bioimaging windows [156].

2.2.10 Anisotropic polarization modulation

The physical and mechanical properties of a single crystalline material often change with different crystallographic orientations. Luminescence from anisotropic crystals often exhibits polarization behavior [157,158]. Polarization can affect the surrounding environment of Ln dopants by lowering the symmetry of the lattice, which can enhance *4f−4f* transition probabilities for enhanced upconversion emission. The polarized upconversion behavior from a single hexagonal-phase $NaYF_4:Yb^{3+}/Tm^{3+}$ microrod was first demonstrated by Qiu and co-workers in 2013 [159]. Under a 980 nm linearly polarized laser excitation, the upconversion luminescence was polarized, and different transitions exhibited the same polarization dependence (Figure 16a and b). By rotating a half wave plate located close to the polarizer, polarized upconversion emission was recorded as a function of the polarization angle, as shown in Figure 16c. Similar observations have been reported in $NaYF_4:Yb^{3+}/Er^{3+}$ nanodisks by the same research team [160]. The linearly polarized laser beam was focused onto two nanodisks with face-up and side-up configurations. The researchers discovered that for the side-up form, the luminescence intensity changes periodically with a sinusoidal dependence on the polarization of the excitation source. In contrast, the upconversion luminescence intensity was independent of the polarization angle in the case of the face-up form. These results reveal that upconversion luminescence varies with light polarization concerning the orientation of the nano-disk under investigation.

In addition to commonly used lanthanide-doped materials, the perovskite oxide materials have also been considered as a candidate host matrix for upconversion luminescence because of low phonon energy. The Han group has reported 43-fold and 8-fold enhancement in the green and red emission of Er-doped $PbTiO_3$ materials [161]. This apparent increase in upconversion emission can be ascribed to the lowering of naturally high tetragonality and polarization of $PbTiO_3$ by the introduction of Er dopants. The tailorable effect of the low-energy E(1TO) phonon will assist in the overall upconversion emission. Moreover, Er^{3+} dopants occupy a Ti^{3+} position with crystal field environment suitable for further adjustment.

2.2.11 High-throughput techniques

Lanthanide-doped upconversion materials exhibit diverse optical properties, which are mainly determined by the combination of Ln dopants, nanoparticle morphology, host matrix, and the surface configuration. However, controlling upconversion luminescence through chemical synthesis with optimal conditions is a very time-consuming challenge due to the dynamic equilibrium between those important parameters. Hence, the development of high-throughput techniques is desirable for rapid screening of experimental parameters suitable for the synthesis of highly efficient UCNPs. Ostrowski *et al.* designed an automated robot for the synthesis of colloidal $NaYF_4$ nanomaterials. They found that the optimal use of ammonium fluoride and oleylamine surfactant could reduce the particle size down to 5 nm [162].

In the previous chapter, we have highlighted the effects of doping combination and concentration on upconversion luminescence. The Chan group has proposed an approach based on microplate-based reactions that include arrays of glass vials arranged in metal blocks. On average, this type of reaction is 24 times faster than conventional methods, while providing additional savings on reagents [163]. Despite the many advantages enabled by the high-throughput method, the search for next-generation UCNPs still relies heavily on conventional techniques. Moreover, the high-throughput

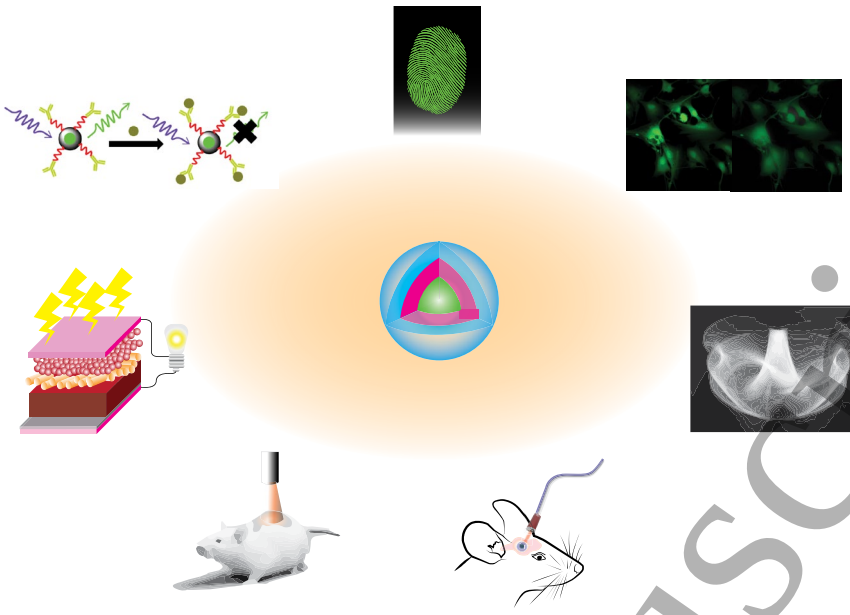

Figure 17. Overview of the emerging applications that capitalize on lanthanide-doped upconversion nanoparticles.

technique may lack flexibility and provide limited information for unraveling the mechanism of upconversion luminescence.

3. Capitalizing upconversion luminescence for emerging applications

A recent development on upconversion research has led to the designing of multifunctional UCNPs for versatile applications in anticounterfeiting, document security, biodetection, super-resolution imaging, photovoltaics, optoelectronics, optogenetics, phototherapies and bioimaging (Figure 17). Given the broad scope of emerging applications, we attempt to provide an up-to-date analysis that could shed light on several critical recent developments of the field.

3.1 Anticounterfeiting and security applications

An analytical approach to identify the accumulation of exogenous and endogenous chemical compounds in latent fingerprints is of utmost value to forensic science as it provides crucial evidence in the criminal investigation and a variety of civil matters. The analysis of forensic databases indicates that friction ridge skin is unique to each individual and does not change over time, meaning that no printed patterns of two fingers or palms are ever exactly alike. As such, this latent fingerprint strategy provides a powerful tool for forensic scientists to identify suspects and victims of crimes and withstand scrutiny in courts of law and public opinion. However, a significant issue arises because the fingerprint development usually necessitates physical or chemical treatments (e.g., dye staining) of the printed area to be examined [164]. At present, uncertainties of forensic evidence due to the lack of a robust stain material pose a significant limitation to daily forensic casework. The utilization of UCNPs may create more sensitive and sophisticated tests, and transform the field of forensic science.

Jin and co-workers prepared a series of UCNPs, dubbed as τ-dots, with tunable lifetimes ranging from 25.6 μs to 662.4 μs [53]. These nanoparticles are not only useful for data security application but also for life sciences (Figure 18a). In their work, the three merged patterns were annotated with various thulium τ-dots of different dopant concentrations, and upon intensity-based luminescence irradiation, a superimposed image appeared. The three encrypted patterns could be decoded by time-resolved luminescence scanning with negligible crosstalk. This approach may potentially open up new avenues for high-density data storage and document security against forgery. The Yuan group constructed a novel aptamer functionalized on the surface of UCNPs that binds specifically to the fingerprint ridges lysozymes [165]. Under 980-nm laser irradiation, a negligible background luminescence was observed, and they demonstrated it is possible to identify cocaine powder-stained fingerprints using the UCNPs modified with a cocaine-binding aptamer (Figure 18b). In another separate work, Kumar and co-workers demonstrated that the Yb^{3+}/Er^{3+} co-doped Sb_2O_3-WO_3-Li_2O ceramic phosphors can generate intense green and red emission under 980 nm laser excitation, which can be used for forensic science, security writing and cryptography information applications [166].

A bright, distinct and low-cost barcode is a highly sought-after target within the community of anticounterfeiting. Liu and colleagues reported the design and synthesis of upconversion microrods that could contribute a valuable addition to the toolbox with multicolor barcodes (Figure 18c top) [167]. Their bottom-up synthetic method can readily access to multicolor-banded microrods with excellent

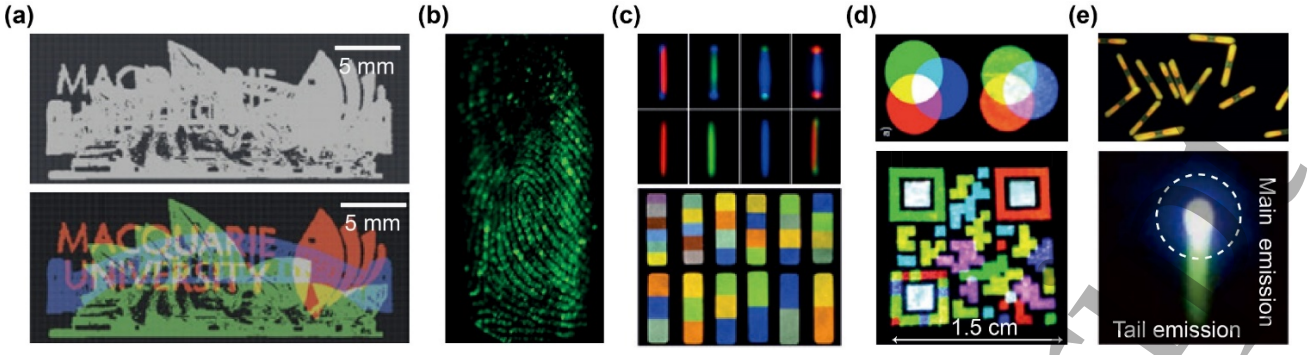

Figure 18. Significant milestones of using multifunctional UCNPs for anticounterfeiting and security applications. (a) Illustration of document security printing *via* lifetime-encoding through the use of three types of $NaYF_4$:Yb/Tm nanoparticles [53]. (b) Application of $NaYF_4$:Yb/Er nanocrystals for latent fingerprinting [165]. (c) Achieving multicolour barcoding *via* single-crystalline microrods: (Top) Optical micrograph photos of dual-colored-band single-crystalline microrods [167]; (Bottom) Luminescence pictures of multicolor microparticles synthesized *via* microfluidic devices [168]. (d) Red-green-blue (RGB) printing of UCNPs [169]. (e) (Top) Upconversion micrographs of the $NaYbF_4$:Er (5 mol%) microrods dispersed on a glass substrate [175] (Bottom) Multilevel anticounterfeiting application using Mn^{2+}-activated core-shell UCNPs that give rise to a bright spot of emission with a green-colored tail upon dynamic laser scanning [176]. Figure reproduced with permission from: (a), [53], Springer Nature; (b), [165], Wiley; (c), Top - [167], American Chemical Society, Bottom - [168], Springer Nature; (d), [169], RSC; (e), Top - [175], Wiley, Bottom - [176], Springer Nature.

crystalline features in gram-scale production. Such an oriented epitaxial growth approach utilizes one-dimensional microrods as the template and affords easy multicolor tuning at a single-nanocrystal level, which is inaccessible by other current approaches. The multicolor-banded microrods would make unique optical barcodes for document security and anti-counterfeiting.

Lee *et al.* designed an encoding system that utilized a multi-scale design approach to access robust encoding. This approach is also amenable to high-throughput particle synthesis, and the encoded information can be easily decoded by a portable charged-coupled device (Figure 18c bottom) [168]. The researchers discovered that the encoding architecture showed significant insensitivity toward particle surface chemistry. They also verified that the decoding error rate was not correlated to the characteristics of the particle material. There is a prospect for direct magnetic manipulation. Their work expanded the potential of manufacturing long-lasting and anticounterfeiting materials with unprecedented encoding capacity from a large collection of exclusively encoded nanoparticles. Another unique work in developing UCNPs for security applications was established by the May group. They utilized an RGB additive color printing system to generate high-resolution pre-defined patterns, which were invisible under ambient lighting but viewable under NIR excitation (Figure 18d) [169].

Surface plasmon modulation is a viable approach to enhance upconversion luminescence. The Song group tapped into the use of Au-Ag alloy/$NaYF_4$:Yb,Tm UCNP composite films for fingerprint identification with unprecedented contrast [170]. The composite films yielded a 180-time enhancement in the overall luminescence intensity relative to the control sample without the Au-Ag alloy. Their work provides unique opportunities to study insights based on the utilization of a hybrid material of metal and upconversion nanoparticles for fingerprint identification applications. Another pioneering work was developed by Li and colleagues, who used an 808-nm laser to excite Nd-sensitized multi-shell UCNPs and generate downshifting infrared luminescence for fingerprint bioimaging [171]. Relative to 980 nm laser excitation, the application of 808 nm laser reduces the overheating effect on the delicate printing substrates.

To safeguard vital security information ranging from currencies to defence intelligence data from being fraudulently used, various strategies and approaches have been developed. These include holographic methods, quick response codes (QR), plasmatic security labels and visible luminescent ink [172]. In recent years, materials such as cadmium telluride (CdTe) and cadmium selenide (CdSe) have been exploited as luminescent security ink. Nonetheless, the intrinsic toxicity of the materials has curbed their widespread applications. By comparison, UCNPs offer down-shifting emission capability, especially in the NIR wavelengths. UCNPs also offer sharp emission peaks, low cellular toxicity, and good dispersibility due to the ease of surface modification. All these attributes make colloidal UCNPs ideal for document security printing [173].

One of the prominent research works was the use of highly luminescent lanthanide-doped nanomaterials by Shanker and co-workers [174]. The uniquely designed enabled dual upconversion and downshifting luminescence modality to be demonstrated using a single 980-nm excitation source. Notably, their work demonstrated a photoluminescence decay time within a few milliseconds, which is appropriate for security applications. Another renowned work was reported by the Wang group [175]. They established a one-pot hydrothermal strategy to access various hollow lanthanide-doped $NaYbF_4$ microrods containing isolated holes along the longitudinal axis *via* kinetic morphology control with facilitation from selective adhesion of citrate ligands (Figure

18e Top). The fundamental mechanistic study showed that the presence of structural void enabled light intensity across the microrods to be altered in the solid matter because of the light scattering and reflection effects within the inner walls. The manipulation of 1D hollow single-crystalline microrods by lanthanide doping can produce complex optical codes upon NIR excitation. Recently, Liu *et al.* illustrated the integration of both long-lived Mn^{2+} upconversion emission and a short-lived lanthanide upconversion in a nanoparticulate system, which enabled the generation of binary temporal codes for active data encoding (Figure 18e Bottom) [176]. By precisely controlling the nanoparticle structure, the researchers verified the excitation usefulness under NIR excitation of both 808-nm and 980-nm irradiation. Interestingly, the researchers discovered that the as-designed Mn^{2+}-doped UCNPs are valuable for multilevel anticounterfeiting with high-throughput authentication rates without the requirement for sophisticated time-gated decoding equipment.

3.2 Biodetection applications

The unique photophysical effects of UCNPs have also been harnessed in various biological studies. One of which is in the area of biodetection. A valuable approach is to take full advantage of resonance energy transfer (RET) using these UCNPs. In RET, the excitation energy is transferred from an energy donor to an acceptor nearby, resulting in diminished luminescence emission intensity of the donor [177]. In recent years, UCNPs have been utilized in many RET-based systems to serve as either energy quenchers or donors. Besides, their large anti-stokes shifts, negligible autofluorescence when irradiated under NIR light excitation and long luminescence lifetimes have been highly useful for RET applications. Tapping into the strengths of UCNPs would increase the performance and allow the prospects of multiple excitation sources to be selected. Undeniably, such RET-based Ln-doped UCNPs can respond with high sensitivity, specificity, rapidly and dynamically to the complex biological environments. Particularly, many organic molecules, biological moieties, metal-organic complexes, and inorganic nanoparticles have been designed and conjugated to the surface of UCNPs for RET-based biodetection.

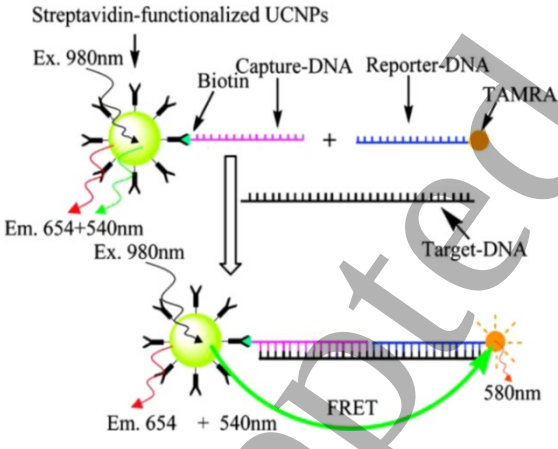

Figure 19. (a) Schematic illustration of the concept of Ruthenium-based complex N719-modified Ln-doped UCNPs and the upconversion luminescence (UCL) response to Hg^{2+} ions followed by addition of KI, which results in a color change in green UCL. (b) UC emission figures and their corresponding merged with bright-field photos of cancerous Hela cells incubated with 0.2mg/ml N719-UCNPs for 3hrs and, (b) Followed by incubation with Hg^{2+} ions for 15 min. Figure reproduced with permission from [178], American Chemical Society.

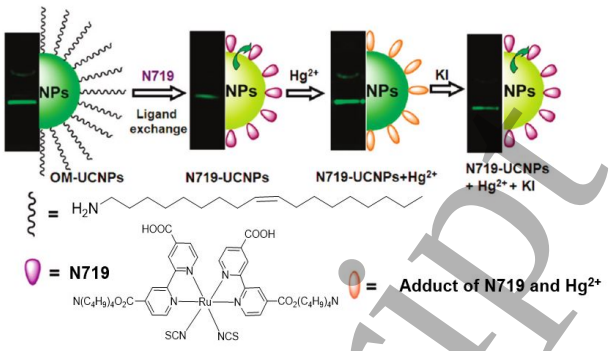

Figure 20. Schematic illustration of the lanthanide-doped UCNPs for mercury Hg^{2+} ion detection. Figure reproduced with permission from [179], American Chemical Society.

An important work in biological detection using UCNPs was reported by the Li and Huang groups. They established a biosensor, based on biocompatible UCNPs, to target and detect a specific DNA sequence [178]. As illustrated in Figure 19, they utilized the specific interaction between biotin and streptavidin to perform RET. The biotinylated DNA sequence was conjugated to streptavidin-coupled UCNPs, with the subsequent addition of a reporter-DNA sequence functionalized with a fluorophore *N*,*N*,*N*',*N*'-tetramethyl-6-carboxyrhodamine (TAMRA). TAMRA has an absorbance that overlaps with the green emission of the UCNPs. By spectrometrically measuring the ratiometric luminescence intensity of (I_{580}/I_{540} or I_{540}/I_{654}), the biosensor can quantitatively identify the concentration of the target DNA sequence. The detection limit is determined to be in the range of nanomole per liter, which meets the sensitivity requirements of routine bioanalysis.

The Li group reported another valuable work for highly efficient luminescence sensing and biodetection. They established a novel absorption-shifting technique involving chemical functionalization of a chromophoric Ru(II) complex onto the surface of $NaYF_4$:Yb,Er,Tm UCNPs *via* a coordination reaction (Figure 20) [179]. These customized nanomaterials allowed the development of a high-selectivity detection tool for sensing mercury ions (Hg^{2+}). Based on ratiometric upconversion luminescence responses, this method registers a detection limit of 1.95 ppb for mercury ions in water, which is lower than the Environmental Protection Agency standard of 2.00 ppb set for drinking water. As an added benefit, these nanoparticles could be used to detect the dynamic change in the distribution of mercury ions in living cells through upconversion luminescence bioimaging.

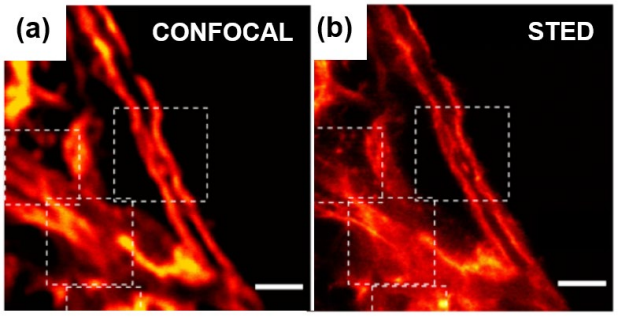

Figure 21. (a) Confocal (b) STED super-resolution images of cellular cytoskeleton labelled with antibody-conjugated 11.8 nm $NaGdF_4$:18%Yb^{3+},10%Tm^{3+} nanocrystals, scale bar represents 1 µm. Figure reproduced with permission from [97], Springer Nature.

The prospects of UCNPs for biodetection through RET can also be used for *in vivo* analyte monitoring. The Li group showed that using a neodymium-sensitized upconversion nanomaterial, a high-contrast probe for the detection of hypochlorite ions (ClO^-) in living cells and arthritis in rodents [180]. The researchers utilized a cyanine dye (hCy3) that is highly sensitive to ClO^- ions. They discovered that the ratiometric upconversion emission of I_{540}/I_{654} could be used to detect ClO^- ions with a detection limit of 27 ppb. Significantly, the feasibility of such tailored-made nanoprobes was ascertained in an arthritis animal model, demonstrating that these UCNP nanoprobes and their associated technology have the potential to be translated and applied for *in vivo* biodetection of vital biological analytes in the future.

3.3 Super-resolution imaging applications

The presence of optical microscopy has evolved tremendously since its first discovery in the 17th century [181]. Even though both scanning-based and electron-based microscopy techniques have overcome the challenges of resolving power, optical microscopy remains an instrumental method for many scientific disciplines. In this context, far-field optical microscopy provides a valuable and unique three-dimensional imaging of biological samples. Besides, the technique offers biomolecular specificity and minimal disruption when fluorescence imaging is integrated [182]. Despite the advantages, a severe constraint is the diffraction limit of light, which limits an optical microscope's resolution to approximately 200 nm. This has serious implications especially when it comes to imaging of molecular structures and intracellular organelles.

The problem of the diffraction limit of light, however, has been overcome in recent years with the advent of several super-resolution methods such as reversible saturable optically linear fluorescent transitions (RESOLFT), photoactivated localization microscopy (PALM), stimulated emission depletion (STED) and stochastic optical reconstruction microscopy (STORM). These highly useful methods have improved resolutions up to the range of 20-nm to 50-nm [183]. Crucially, the recent popular STED method utilizes stimulated emission to reduce the spontaneous fluorescent emission of materials that fluorescent to the central sub-region of an observation volume *via* de-excitation of fluorophores in the periphery regions. This was done by overlapping a focused excitation beam with a "doughnut"- a shaped beam that de-excites emitters to the ground state with the exception for the plane by reducing the full-width at half-maximum (FWHM) of the point spread function [184,185]. The area within the boundaries of the center of the doughnut can render unlimited high resolution in the transverse plane and thus enable super-resolution imaging.

In the context of super-resolution imaging applications, UCNPs signify an entirely new class of multiphoton luminescent probes. Their luminescence intensity hinges on the concentration of the multiphoton emitters that are localized within the miniature nanoparticles. Recent research demonstrated that thousands of emitters embedded in each nanoparticle could be stimulated by high power laser pumping to generate bright luminescence, which offers an attractive and promising single-particle-based nanoprobe [186,187]. These highly concentrated dopants in UCNPs render seamless optical population inversion at their intermediate energy metastable levels [95]. Consequently, a minimal saturation intensity of approximately 0.19 MW/cm^2 in upconversion STED was documented with a maximum threshold resolution of 28 nm (λ/36) for optical imaging of a single nanoparticle of 13 nm in diameter. Of significance in super-resolution imaging would be the work by Jin and co-workers, who established UCNPs with unusually high doping concentrations of thulium ion (Tm^{3+}) to attain low-powered super-resolution STED microscopy [95]. Two UCNP samples were prepared with an average size of 39.8 and 12.9 nm and co-doped with similar dopant compositions of 8% Tm and 20% Yb prior to the STED microscopy. Under 808 nm laser irradiation of 9.75 mW/cm^2, a 48.3-nm spot FWHW was attained from 39.8 nm UCNPs while a 13-fold enhancement over the optical diffraction limit was measured by FWHM after Gaussian fitting analyses (Figure 8e). On the other hand, a 31.2 nm spot FWHM was seen from the 12.9 nm UCNPs, and a similar high contrasting improvement in resolution was discovered relative to traditional confocal imaging studies. Remarkably, their results demonstrated that utilizing low-powered laser radiation on UCNPs may effectively overcome the overheating problem that limits the widespread utility of super-resolution imaging for bioanalysis.

Another notable work was demonstrated by He and colleagues, who tapped into the intrinsic cross relaxation between the lanthanide dopants embedded within the UCNPs to generate a supplementary route for optical depletion of blue emission at 455 nm using highly doped Tm^{3+}-$NaYF_4$:Yb^{3+}/Tm^{3+} with improved interactions between adjacent thulium ions [97]. This resulted in a near complete silencing of blue emission using the induced stimulated emission from a second laser beam source and concurrently obviated the enhancement effect of the same laser beam. Such

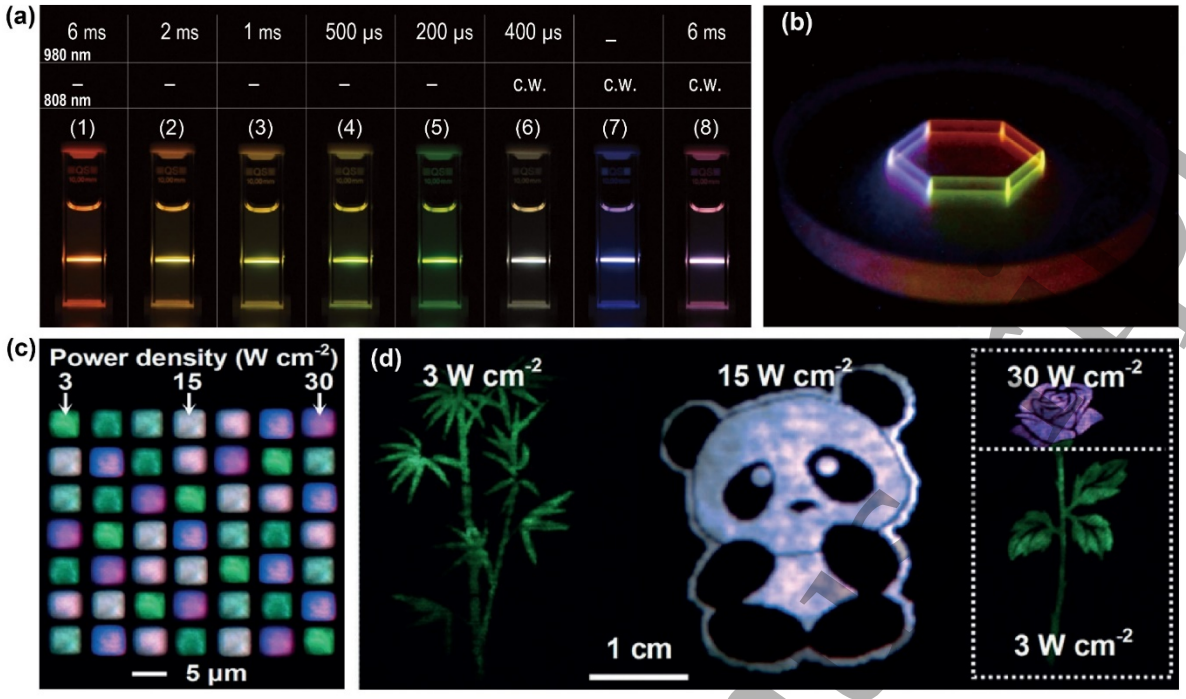

Figure 22. Multicolor upconversion nanoparticle on display. (a) Luminescence photos illustrating multi-color tuning of the sample utilizing the combination of both NIR lasers. (b) Demonstration of volumetric full-color three-dimensional display generated *via* the use of the designed multi-layer upconversion nanoparticles. Scale bars, 1 cm. (c) A dot-array image on silicon wafer and Ln-doped UCNPs were loaded inside a 5 by 5 μm etched microwells on a silicon wafer. (d) Photos of bamboo, panda and rose printed on paper with an inkjet printer using the synthesized nanoparticles as colourless ink. Figure reproduced with permission from: (a-b), [93], Springer Nature; (c-d), [94], John Wiley and Sons.

an innovative emission depletion strategy is amenable to super-resolution microscopy and facilitates nanoscopic cytoskeleton imaging at high speed (100 μs dwelling time) with super-resolution imaging of cellular cytoskeleton protein structures with a resolution of 80 nm (Figure 21a and b).

3.4 Display applications

The eventual goal in encoding and modulating colors in material science research is to realize a universal sensitive and responsive material which has the potential to be accessed remotely on demand using external stimuli. These can range from pressure, magnetic, light and electric fields. Of importance, these useful optical materials can potentially be translated into displays that possess higher resolution than achievable by the existing red-green-blue (RGB) pixilated color display methods. Significantly, both two-dimensional pixelated RGB and three-dimensional volumetric full-color displays require the mixing of individual RGB elements as one color pixel which is necessitated by the specifications for devices with unique pixel manufacture and configuration [93]. Given the multitude of fundamental studies on color tuning strategies in lanthanide-doped nanomaterials that have been addressed, it is without a doubt that they can represent the next generation of luminescent materials for display technology applications. One of the attractive features of these nanomaterials is the possibility to modulate emission color under a single wavelength excitation. This can be achieved with a high spatial resolution by controlling the intensity ratio of emission peaks [188].

Deng *et al.* showcased a dynamic fine-tuning emission of core-shell lanthanide-doped nanomaterials to generate the entire visible wavelength range and have the grand possibility to manufacture truly three-dimensional full-color display devices with high spatial resolution and locally addressable color gamut for commercialization [93]. We discovered and attributed to the ability to attain such unique and superior luminescence via tuning the pulse width of NIR laser beams (Figure 22a). The lanthanide-doped nanoparticles were synthesized *via* an epitaxial layer-by-layer approach with low phonon β-hexagonal phase $NaYF_4$ as the host structure, and five groups of activated lanthanide ions (Tm^{3+}, Yb^{3+}, Nd^{3+}, $Ce^{3+,}$ and Ho^{3+}) were doped into several layers to afford color-tunable multi-shell nanoparticles. The incorporation of these designed lanthanide-doped nanoparticles into polydimethylsiloxane (PDMS) monolith to manufacture a transparent display and a conceptual proof of multi-perspective color images with the immense resolution was achieved by laser excitation with both 980-nm and 800-nm (Figure 22b). Crucially, equal mixtures of each Ln-doped UCNPs with balanced monochromatic RGB elements over a solution or solid-state substrate can emit white color.

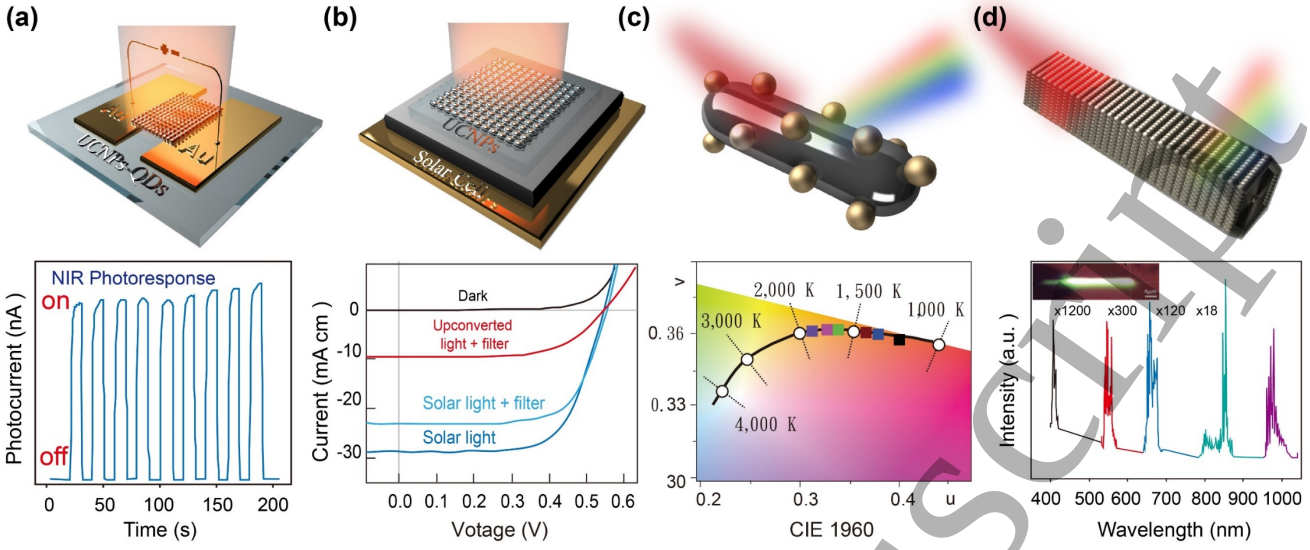

Figure 23. UCNPs for optoelectronic devices and photovoltaic applications. (a) (Top) A novel nanoheterostructure consisting of lanthanide-doped upconversion nanoparticles with CdSe quantum dots (QDs) termed as CSNY. (Bottom) The reversible on-off switching characteristics profile upon 980-nm excitation. (b) (Top) An electronic device by assembling two contact devices *via* a spin-coating solution of CSNY particles in solution onto Si/SiO_2 substrate pre-patterned with gold electrodes. (Bottom) A graph depicting current density–voltage curves of the Si solar cell under AM1.5 solar light (blue) with the short-pass filter (cyan), under the upconverted white light with the short-pass filter (pink) and in dark (black). The upconverted white light came from 28 mol% Yb^{3+}-doped ZrO_2 under 976-nm laser excitation. (c) (Top) A unique nanoheterostructure nanorods consisting of lanthanide-doped upconversion nanoparticles $(Gd,Yb,Er)_2O_3$ with AuNPs. (Bottom) Temperature mapping in the form of a CIE 1960 (u,v) chromaticity diagram, generated by using Au particle-modified Gd_2O_3:Yb,Er nanorods. The similarity of emission location with the Planckian locus (curved line with circles) enables temperature mapping from 300–2,000 K. (d) (Top) A schematic diagram showing the designed NIR upconversion lasing using single-crystal Er-Y chloride silicate nanowires. (Bottom) The upconverted light emission spectra from 400-nm to 1000-nm of the Er-Y chloride silicate nanowires upon excitation at 1480-nm. Insert: Optical image of the pumped nanowire. Figure reproduced with permission from: (a), [87], American Chemical Society; (b), [151], Springer Nature; (c), [190], Wiley; (d), [191], Springer Nature.

Another notable display application using lanthanide-doped nanomaterials was reported by Zhang's group [94]. In their research, they established an upconversion nanomaterial system which can generate RGB emission colors that include the entire electromagnetic visible spectrum and when mixed together, they can produce white light (Figure 8d). Significantly, by simply tuning the excitation power density, they showed that the upconversion emission colors could be changed. This auxiliary strategy can be amenable to display technological applications *via* modulating the output of the emission colors through a facile excitation source. They designed a lanthanide-doped nanoplatform in which six different lanthanide dopant ions were doped (Tm^{3+}, Yb^{3+}, Y^{3+}, Er^{3+}, Gd^{3+}, and Eu^{3+}). They showed that upon irradiation by 980-nm NIR laser, origins of blue light was generated by Tm^{3+}, green light by Er^{3+} and red light by Eu^{3+} dopant ions were observed. Surprisingly, they discovered that the emission colors could be dynamically modulated by changing the 980-nm laser excitation power density, which from the range of 3 to 30W/cm^2, showed a color evolution from green to cyan to white and finally to red. Crucially, this discovery was similarly observed when the colloidal nanocrystals were incorporated into the polystyrene microbeads. As a proof-of-concept, the authors developed a prototype flat-panel display that contains the designed lanthanide-doped nanocrystal-coated substrate, and it can generate different emission visible colors *via* a rapid scanning laser that is synchronously tuned by modulating the pump current (Figures 22c and d).

3.5 Photovoltaic and optoelectronic applications

Photovoltaic which is also known as solar cells are semiconductor devices that create electricity *via* transforming solar radiation directly into electricity through the photovoltaic effect [12]. Notwithstanding, the main issue in the widespread application is the efficiency in energy conversion because they are only responsive to a small fraction of solar photons with photonic energy higher than the threshold bandgap of the system. As such, there are inherent fundamental disadvantages in maximizing the efficiency threshold of these solar cells. To further enhance such conversion efficiency, a promising strategic approach is to tap onto lanthanide-doped upconversion nanomaterials to establish productive spectral conversion because of the rich multiple energy level structures native to the lanthanide ions. This would enable simple photon management useful for photovoltaic applications [5,189]. Since they have the potential to convert two or more sub-bandgap NIR photons

into one usable above-bandgap photon, it is also highly valuable as this can reduce non-absorption energy losses in various photovoltaic devices [12].

One of the emerging photovoltaic applications is the use of multicomponent heterostructures that comprises two or more nanoscale components organized in a structured way that was reported by Perepichka and co-workers [87]. They discovered that the interaction between the integrated components could tremendously enhance the intrinsic electronic properties and developed a heterostructured nanosystem that blends UCNPs with CdSe quantum dots – CdSe/$NaYF_4$:Yb/Er (CSNY). This hybrid nanosystem which comprises both upconverting and semiconducting properties gave rise to sub-band-gap photoconductivity. The research team illustrated the utility of CSNY photoconductivity in electronic devices by assembling two contact devices *via* a solution spin-coating of CSNY particles onto a silicon substrate pre-patterned with gold electrodes (Figure 23a Top). Upon 980 nm irradiation, the upconverted photons generate excitons and further create charge carriers within the CdSe-based films. Consequently, a reversible and durable NIR photoconductivity switch is achievable as exemplified in the photocurrent-time graph (Figure 23a Bottom). Significantly, this novel concept currently devised for microelectronics can be applied in photovoltaics to accumulate photons with sub-bandgap energies.

In another important work, Wang *et al.* showcased a photon energy upconversion *via* the thermal radiation route that resulted in the highest power upconversion efficiency achieved around 16% [151]. They introduced various lanthanide and transition metals as sensitizers into oxide hosts in order for the absorbed infrared photons to be transferred to the host lattice structure through multiphonon relaxation. As such, the accumulation of phonons in the host lattice increases the temperature and exacerbates the thermal radiation, in which a vast number of photons possess higher energy than the incident photons. Importantly, this strategy leads to relatively high upconversion efficiencies. With an optimal design comprising 28 mol% Yb^{3+} dopants, they achieved an upconversion power efficiency of 16% under continuous wave 976-nm laser excitation (Figure 23b Top). Of importance, they showed the practicability of using both concentrated sunlight and continuous wave 976-nm laser source to generate upconverted white light. The white light produced is further absorbed by silicon solar cells to create useful electrical energy that can drive optical and electrical devices (Figure 23b Bottom).

The concept of light-induced thermal heating of various noble metal nanomaterials has been a strategic approach for many applications in recent years. This is especially true in photovoltaic and plasmonic research. An appealing work on plasmonic-induced nano-heaters was reported by Carlos and co-workers, who developed an all-in-one heterostructures nanothermometer comprising a lanthanide-doped oxide material $(Gd,Yb,Er)_2O_3$ for temperature sensing and surface-tethered gold nanoparticles as heaters. Their design enabled an

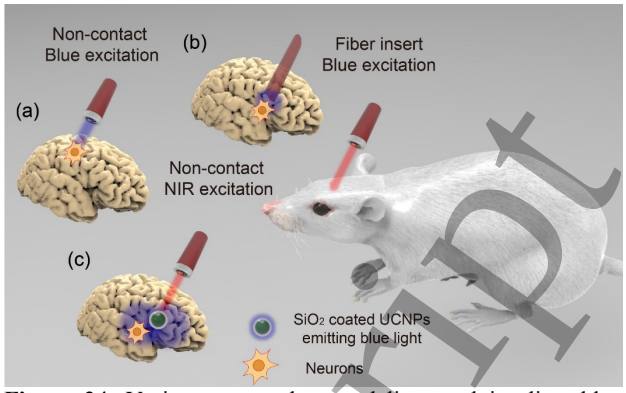

Figure 24. Various approaches to deliver and irradiate blue excitation light to the neurons that are found deep-lying in the mouse brain. (a) Low efficiency of blue light excitation *via* the non-contact blue excitation due to light scattering. (b) A surgical invasive implanted optical fiber to generate blue light excitation to modulate the neurons but restricts the movements of the mouse's movements and can result in surrounding brain tissue damage. (c) An optimal non-contact NIR-to-Blue visible light excitation *via* the use of UCNPs to modulate the function of neurons.

ultrasensitive nanothermometer covering a wide temperature range from 300 – 2000 K (Figure 23c Top and Bottom) [190]. In their work, heat generation was produced by AuNPs upon 980 nm excitation. Their material utilized the ratiometric intensities derived from Er^{3+}-upconverted green and red emissions at a temperature range of 300 to 1500 K. Remarkably, with an increasing amount of AuNPs, they discovered that both surface temperature and operating range of the nanothermometers increased. They attributed the white-light emission to an incandescence process. The thermal-sensing principle was discovered in close association with the cooperative effect of thermal equilibrium in the population of excited states on Er^{3+} upconversion nanorods. This work not provides many prospects for photovoltaic research but also raise the possibility for controlled hyperthermia and deep-tissue tumor imaging without causing overheating damage to adjacent normal tissues.

Another intriguing work for optoelectronic devices operating at NIR wavelength was reported by Ye *et al.*, who synthesized a new upconversion lasing based on Erbium-Yttrium chloride nanowires (Er-Y) (Figure 23d Top) [191]. They demonstrated that upon 1476-nm laser irradiation on a single-crystal Er-Y chloride nanowire, an ultra-narrow linewidth of 980 nm lasing was observed with a well-resolved sharp emission line (0.25nm at 77K) within the wavelength range of 400-nm to 1000-nm (Figure 23d Bottom). Besides, they showed that at the highest Er/Y ratio in these nanowires would result in a blue shift of the strongest peak. Importantly, the ability to generate 980-nm lasing properties of these ER-Y chloride nanowires upon irradiation by 1476-nm would enable their utilization to attain tunable NIR laser and have prospects in nanoscale optoelectronic devices that can perform at NIR wavelengths.

3.6 Optogenetics applications

UCNPs have also conjured considerable attention in potential biological applications. When compared to traditional luminescent probes such as quantum dots, fluorescent proteins or organic dyes, UCNPs have superior photophysical properties such as resistance to photobleaching, non-photoblinking, non-autofluorescence and the lack of cross-talked emissions [189]. The use of NIR excitation source also enables deeper tissue penetration than achievable with UV and visible range excitation typically reserved for conventional bioimaging probes. One of the most important strengths of UCNPs is that a low power continuous-wave laser operating at a power density of (1-1000 W/cm^2) is sufficient to initiate the photon upconversion process [192]. Owing to their unusual photophysical behaviors, UCNPs provide scientists with a powerful tool to unravel the mysteries of life sciences in areas such as optogenetics [193,194], photodynamic and photothermal therapies [195,196]. Also, the down-shifting ability of the UNCPs is highly valuable since the down-shifting emission can be tuned into the second biological window where minimal biological tissue scattering occurs [197].

The development of advanced optical tools and devices has revolutionalized the field of optogenetics and enabled a precise control over the activity of neurons with light. This intriguing field uses genetic engineering methods to selectively insert opsins and its related family of proteins such as halorhodopsin, bacteriorhodopsin, and channelrhodopsin into randomly marked sub-population of neurons in the brain [198]. Upon irradiation with light *via* fiberoptics or other light-guiding instruments, those marked neurons can be modulated to activate or deactivate with millisecond timing [199-201]. The ultimate goal of optogenetics is to allow scientists within the neuroscience field to harness the use of optical control of these neurons in various organism models and design novel therapeutics to treat neurodegenerative diseases.

Experimental studies have shown that it is possible to modulate the biological activities of light-gated and light-driven ion pumps found in opsins using the visible light in the spectral range of 430 nm to 630 nm [202]. There is a possibility that a cascade of events due to light exposure allows genetically engineered neurons to be activated or inhibited. Nonetheless, direct blue light excitation has limited tissue penetration depth due to severe light tissue scattering (Figure 24a). Fiber insertion can overcome the problem of tissue penetration, but this approach may restrict the freedom of movement of the animals under study, usually mice or rats, and result in tissue damage during experimentation (Figure 24b). A considerable research effort has gone into extending the wavelength excitation toward the red and NIR region because of the intrinsic deeper tissue penetration at these wavelengths. However, the design of genetically coded opsins responsive to the red and NIR region presents a substantial challenge. A promising strategy to overcome this limitation is to tap onto the nanotransudcing capabilities of UCNPs, which

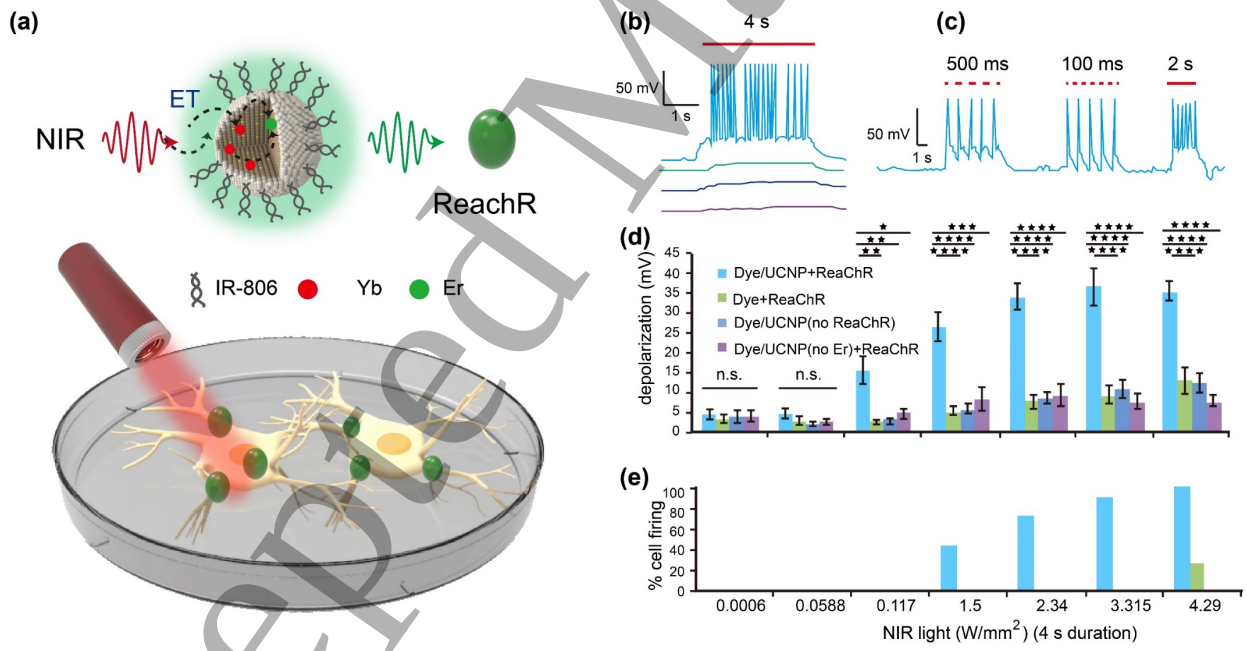

Figure 25. The design and crucial experimental results of the Ln-doped UCNPs in [193]. (a) Schematic illustration of the rationally designed novel IR-806 dye-sensitized core/shell lanthanide-doped upconversion nanoparticles (β-$NaYF_4$:20%Yb^{3+}/2%Er^{3+}@β-$NaYF_4$:10%Yb^{3+}) for NIR-activated optogenetic application to control the red-activatable channelrhodopsins (ReaChR) *via* 800-nm laser excitation. 800-nm activation of ReaChR in the designed cultured hippocampal neurons. Electrophysiology graphs demonstrating the potential firing in response to (b) Prolonged – 4s, (c) Pulsed (100ms, 500ms and 2s) delivery at (2.34 W/mm^2) (d) Neuronal depolarization and (e) Action potential firing triggered by 800-nm NIR laser excitation at various intensities for 4s. There can be neuronal activation and depolarization in some control cases. Figure reproduced with permission from [194], American Chemical Society.

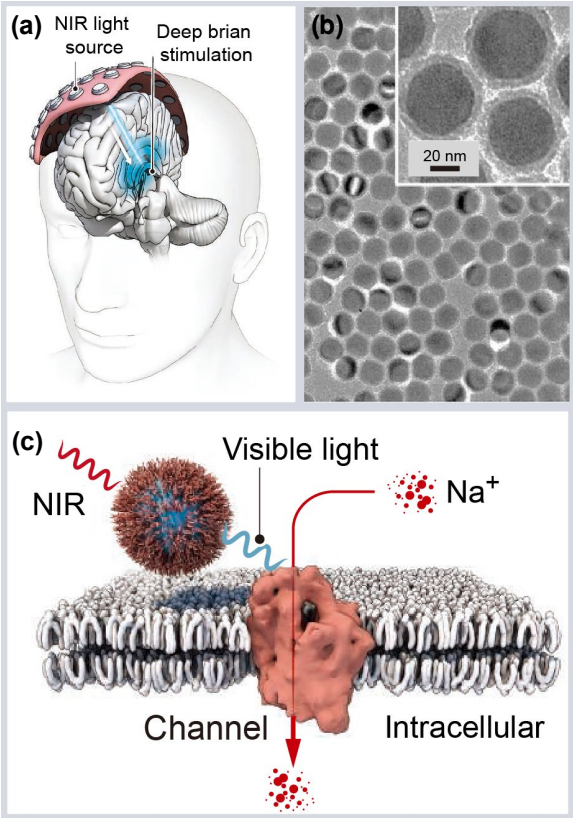

Figure 26. (a) Schematic figure of a typical light source array for deep-seated brain stimulation optogenetic applications. (b) TEM diagram of surface-modified lanthanide-doped nanoparticles. Insert: A close-up magnification of the corresponding as-synthesized silica coated lanthanide-doped nanoparticles. (c) Schematic illustration of the rationally designed surface-modified lanthanide-doped UCNPs for UCNP-assisted NIR upconversion optogenetics application. Figure reproduced with permission from [193], The American Association for the Advancement of Science (AAAS).

can convert NIR laser stimulation into UV/Visible output (Figure 24c) [189,203].

A notable optogenetic demonstration through the use of UCNPs was reported by the Han group in 2016 [194]. The researchers developed a state-of-the-art IR-806 dye-sensitized core-shell nanoparticles that feature a broad absorption range and an enhanced luminescence efficiency due to the conjugation of IR-806 antenna to the particle's surface (Figure 25a). In the absence of an invasive procedure of embedding optical fibers, they demonstrated the ability to control the neuronal activity in cultured hippocampal neurons that expressed red-activatable channelrhodopsins (ReaChR) upon excitation with an 800 nm laser. (Figure 25b-e). Significantly, the as-synthesized Ln-doped UCNPs demonstrated good water solubility with Pluronic F127 for used in future bioimaging applications.

One of the recent works on NIR-based optogenetic manipulation was reported by Chen *et al.*, who demonstrated that UCNPs could serve as optogenetic actuators for transcranial NIR light stimulation of deep brain neurons (Figures 26a-c) [193]. The proof-of-concept was achieved by utilizing transgenic mice infused with UCNPs to locally activate light-gated ion channels and modulate neuronal activity, deep inside the brain of the mouse. Remarkably, this led to stimulation of brain oscillations *via* activation of inhibitory neurons in the medial septum, silenced seizure through blocking the hippocampal excitatory cells and enabled memory recall through hippocampal engram experiments. Most importantly, the researchers demonstrated that an exceptional nano-transducer capable of converting deep tissue NIR laser irradiation to blue light could enable fast increases in dopamine release in the deep brain and raise the possibility of using such UCNP-mediated neuronal modulation tools to mitigate neurological disorder that has yet been successfully addressed at the present moment.

3.7 Phototherapy and bioimaging applications

UCNPs have also found its prospects for phototherapies and diagnostic bioimaging. Phototherapies include photodynamic therapy (PDT) and photothermal therapy (PTT). UCNPs photoactivate the photosensitizers by converting NIR laser irradiation to visible light, which can be used to generate lethal cytotoxic reactive oxygen species (ROS) [204]. This approach is highly efficacious and has been used for a range of cancer treatments because of the minimal chronic cellular cytotoxicity of the nanomaterials, the accurate targeting capability of the laser source, and the low cost needed for experimental setup [195].

Liu and co-workers developed Ce6-modified UCNPs (Ce6: chlorin e6) and discovered that the NIR light could permeate an 8 mm thick pork and yield noticeable PDT cellular effects to reduce tumor growth rate (Figure 27a) [205]. Another similar work for effective treatment of tumors was reported by the Gu group, who developed a ZnPc photosensitizer-based upconversion system (ZnPC: zinc phthalocyanine) (Figure 27b) [206]. Zhang and co-workers developed a dual-sensitizer system (ZnPc: zinc phthalocyanine and MC540: merocyanine 540), in combination with Er^{3+}-based UCNPs for the generation of both green and red emissions under irradiation at a single NIR wavelength, for mouse cancer models. This protocol enables effective noninvasive deep-tissue cancer therapy (Figure 27c) [207]. The same group also achieved another notable milestone in PDT application in which they developed titania-coated UCNPs (Figure 27d) [208]. The limited loading efficiency of photosensitizers was overcome by replacing the organic photosensitizers with a uniformly coated titanium dioxide (TiO_2). Through doping with Tm^{3+} ions, the upconverted UV light would photoexcite the electrons occupying the valence band of TiO_2 and promote them to the corresponding conduction band. This band transition leads to the generation of electron-hole pairs and evokes redox reactions with molecular oxygen and water to produce reactive oxygen species and leads to tumor cell death.

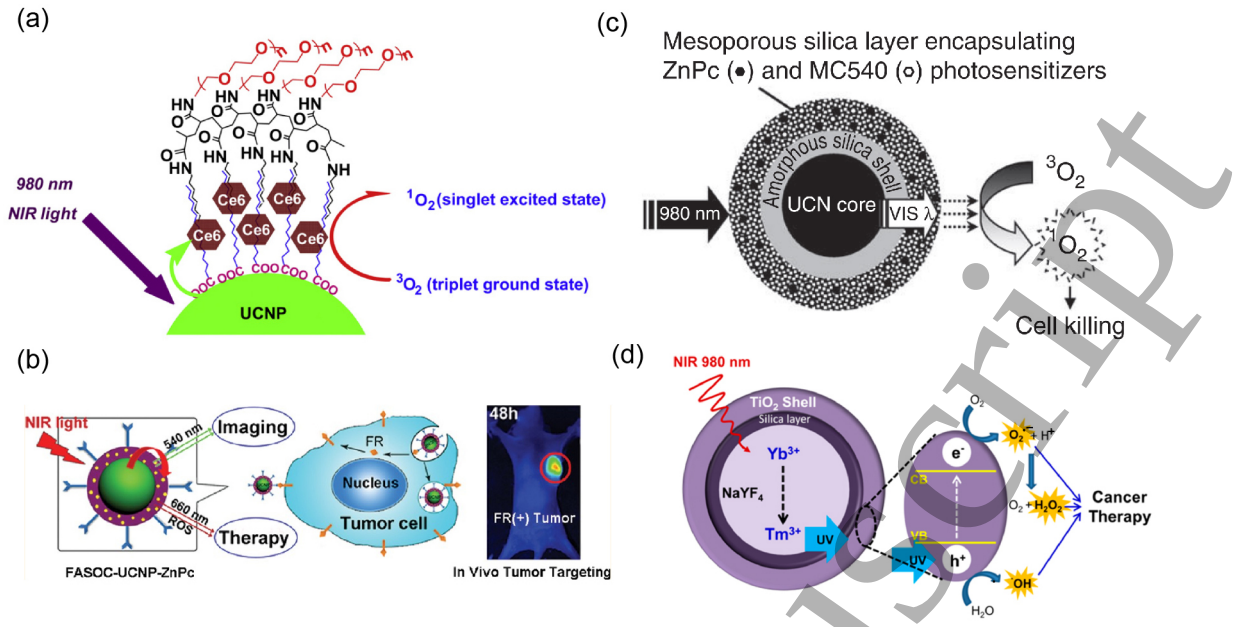

Figure 27. Various emerging NIR excitable Ln-doped UCNPs for Photodynamic Therapy (PDT) (a) A diagram showing NIR-induced PDT which has Ce6 functionalized onto the Ln-doped UCNP. (b) A figure illustrating the tumor-targeted Ln-doped UCNP using ZnPc and applied for *in-vivo* tumor PDT. (c) Figure showing the as-synthesized mesoporous-silica coated Ln-doped UCNPs doped with Er^{3+} and co-loaded with MC540 and ZnPc photosensitizers. Upon 980-nm irradiation, red and green visible upconverted light were generated and activated the photosensitizers to generate ROS. (d) A novel NIR-to-UV TiO_2 coated-Ln-doped UCNP for uniform and effective ROS generation in which UV light photoexcites the electrons from the valence band to the conduction band in TiO_2 shell. This results in photoinduced electron-hole pairs and the interaction of native triplet molecular oxygen and water molecules would lead to generation of various ROS and cause cancer cell death. Figure reproduced with permission from: (a), [205], Elsevier; (b), [206], American Chemical Society; (c), [207], Springer Nature; (d), [208], American Chemical Society.

Another useful phototherapy would be photothermal therapy (PTT). This noninvasive therapeutic approach employs photothermal agents to absorb light for heat generation, the subsequent denaturation of the proteins found inside the cells, and ultimately the cell death. It can also result in thermal ablation of cancers [204]. This strategy creates several advantages such as being selective and accurate since it relies on the spot where the laser is irradiated, and only those regions covering the photothermal agents would result in temperature rise. Also, similar to photodynamic therapy, PTT can be considered flexible and cost-effective for potential efficacious treatment against cancer. In the context of UCNP-based PTT application, the UCNPs are usually mingled with other types of photothermal agents that possess a high extinction coefficient, such as gold, transition metal sulfide or indocyanine green, or even polydopamine, because of the intrinsic low extinction coefficient of lanthanide ions.

One of the UCNP-based PTT demonstrations is the work developed by Song and co-workers, who reported the fabrication of a multifunctional Ag-UCNP nanocomposite. Due to surface plasmon resonance absorption at 980 nm, the excitation energy can be harvested by the outer silver shell and efficiently transfer to UCNPs. The intelligent design led to its utility for photothermal ablation of human liver and breast cancer cells [209]. Another outstanding work was published by Liu and co-workers, who designed and synthesized a layer-by-layer assembly of core-shell nanocomposite [210]. The nanocomposite comprises an UCNP core, a layer of iron oxide nanoparticles serving as the intermediate shell, and an outermost shell layer of gold nanoparticles (Figure 28a). Remarkably, the amount of nanocomposite that localized in the tumor tissue regions upon manipulation of an external magnetic field was about 8-times higher than that obtained with the control group without applying the magnetic field. Owing to the large optical absorption coefficient of gold nanoparticles in the NIR range, near complete thermal ablation of tumors in mice was achieved when irradiated with a NIR laser. This resulted in maximum life-span for the mice under study (Figures 28b and c). Hence, the nanocomposite could provide a platform to enhance the efficiency of thermal ablation, with the assistance from an external magnetic field for magnetic targeting and a dual-imaging modality consisting of magnetic resonance imaging and upconversion bioimaging.

In another example of PTT demonstration, Hilderbrand and co-workers developed a hybrid system comprising UCNPs and carbocyanine organic dyes [211]. They synthesized Er^{3+}-based UCNPs with a thin layer of silica coating, and the carbocyanine dyes were encapsulated within the silica layer (rephrase). When subjected to 980-nm laser irradiation, superior cellular imaging was observed. With 750 nm laser irradiation for 2 minutes at 2.5 W/cm^2, the temperature of the nanostructures increased by 21°C. They showed that about 42% of murine leukemia (RAW) cells were thermally killed, demonstrating the efficacy of PTT treatment.

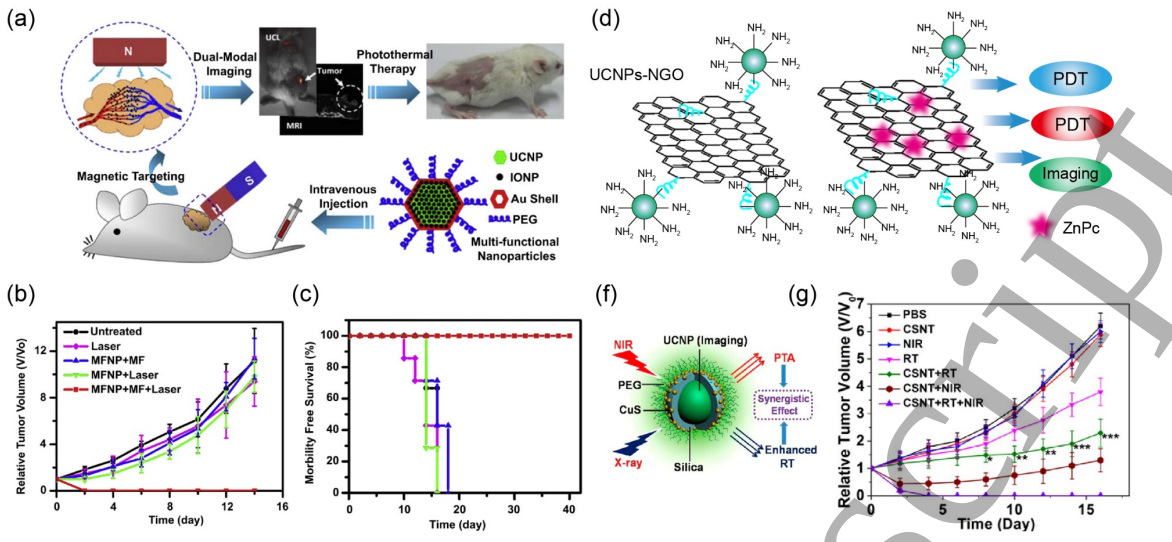

Figure 28. A collection of photothermal therapy (PTT) applications integrating NIR excitable UCNPs. (a) A diagram showing the composition of the as-synthesized nanocomposite and the conceptual workflow for the *in vivo* image-guided magnetic targeting PTT application in a mouse tumor model. (b) *In vivo* magnetic targeted PTT profile and the growth of 4T1 tumors in various groups of the mice upon treatment with various control groups. (c) The representative survival curves of mice bearing 4T1 tumors after various therapeutic control groups [210]. (d) Schematic figure showing the UCNP-nanographene oxide (NGO) nanocomposite in which the NGO was grafted with the UCNPs through bifunctional polyethylene glycol (PEG). (e) The intrinsic multifunctional theranostic features of the designed UCNPs-NGO/ZnPc nanocomposites [214]. (f) Schematic figure showing the Ln-doped UCNP-CuS-PEG nanocomposite and possess trimodal imaging with dual synergistic photothermal and radiation therapies [214]. Figure reproduced with permission from: (a-c), [210], Elsevier; (d-e), [214], Elsevier; (f-g), [215], American Chemical Society.

To further enhance the therapeutic efficacy, researchers continue to explore and develop multifunctional nanomaterials that combine several functionalities into one heterogeneous system. This paradigm shift was proposed to overcome the multi-drug resistance and recurrence of the tumor due to its intrinsic nature of complexity and heterogeneity [212]. As such, the possibility of incorporating multiple therapeutic modes within UCNPs has continued to progress in this direction in the hope to develop a more effective nanoplatform with minimum side effects [213]. For instance, the Zhang group demonstrated an interesting work showcasing this multifunctional concept. They synthesized poly(allylamine)-coated UCNPs, covalently conjugate them with graphene oxide, and subsequently attached ZnPc photosensitizers to the surface of the graphene oxide (Figure 28d) [214]. In this system, the graphene oxide with absorption at 808 nm functions as the photothermal agent to provide PTT while the ZnPc absorbs at 630 nm to generate ROS such as cellular cytotoxic singlet oxygen $^1O_2$. The researchers demonstrated the synergistic interplay between PDT and PTT, which gave rise to an enhanced therapeutic efficacy on those labeled cancer cells (Figure 28e).

In more recent work, Xiao *et al.* developed a trimodal therapy that combines image-guided synergistic photothermal treatment and X-ray radiation [215]. In their work, they consolidated silica-coated a $NaGdF_4$:Yb,Er nanoparticle and CuS nanoparticles into a hybrid nanocomposite (Figure 28f). The proof-of-concept of radiation therapy was validated by exposing the nanocomposite to high energy X-ray irradiation. The versatile imaging capabilities of the nanocomposite, namely photon upconversion, magnetic resonance, and computed tomography, led consistent inhibition of tumor growth when subjected to PTT under *in vivo* conditions (Figure 28g). The application of this radiation therapy to 4T1 tumor resulted in a total ablation after four days, and no tumor recurrence was observed during a longitudinal 120-day experimental study.

4. Outlook and perspectives

Photon upconversion in lanthanide-doped UCNPs has drawn much considerable attention, as highlighted in this review and elsewhere, over recent years. Many fundamental studies, as well as a diversity of emerging applications, have been demonstrated using these luminescent nanomaterials. These examples illustrate the promising prospects for commercialization and translation for various industries. With a repertoire of experimental methods available to tune photon upconversion, either through chemical or physical strategies as outlined in this review, these nanomaterials have the potential to transform many fields of research.

Worth mentioning would be the characteristics of UCNPs. They are amenable with ease to surface deposition as layered films from solutions. Furthermore, for microelectronic application, the reorganization of the films is adaptable with traditional lithographic steps because of the high thermal stability and photostability of these nanoparticles. UCNPs can also be directly molded using a flexible elastomeric stamp.

Their unique photophysical and photochemical properties make them ideal for biological applications such as bioimaging and photothermal therapy. For those optogenetic and super-resolution imaging applications currently in development, the present achievements by various research groups are indeed encouraging. For example, the recent optogenetic research appears to suggest that neural circuitry optical modulation by UCNP-assisted optogenetics have proven effective in the remote interrogation of genetically modified neurons with high spatial resolution and sensitivity.

Nonetheless, UCNPs have several inherent limitations. First and foremost, their low upconversion quantum yield, usually less than 1%, may limit their widespread use in various applications. Thus, a major challenge in materials chemistry is to boost the quantum yield. At present, the highest quantum efficiencies measured for NIR-to-visible conversion are about 5% for irradiation power densities of less than 100 W/cm^2 [216,217]. A few approaches can be implemented to enhance radiative rates in these lanthanide-based upconverters. One effective strategy is to use organic dyes as sensitizers [218]. Other methods include host-lattice manipulation, energy transfer modulation, surface passivation, and photonic crystal engineering. Another research challenge is to address the possibility of unconventional excitation wavelengths instead of the traditional 808-nm and 980-nm NIR excitation source. A feasible approach is to tap onto organic dyes, which can serve as antennas and guide the energy transfer to the lanthanides embedded in the host lattice.

There is also the need to design and build instruments in parallel that enable a critical evaluation of UCNPs for their translational value. At present, the implementation of research works in this field often requires a customized microscopic or spectroscopic setup where a specific NIR laser source is frequently not available with commercial equipment packages [219]. As such, there is a huge unmet need for easy accessibility of commercial equipment that would benefit many research groups. This advancement would improve the robustness and reproducibility of the results such as quantum yield, lifetime measurement, and spectroscopic measurements.

Another pivotal area worth investigating in upconversion research would be gearing these nanomaterials toward translation applications for industries. Well-established and routine synthetic pathways and rational surface engineering approaches of the UCNPs are crucial and form the basis for commercialization. These methods have to be comprehensively verified using various physicochemical and photophysical techniques, much like the quality assurance checks performed on manufactured drugs in pharmaceutical industries. Establishment and regulation of standard protocols for sturdy surface modifications with various biomolecules is of utmost importance. Besides, complementary to the synthesis strategy are the novel techniques afforded in the bioconjugation chemistries, which would result in high quality and high-performance nanomaterials for advanced research.

A parallel effort would be the rational and thorough examination of the long-term chronic toxicity studies of UCNPs in biological media, especially those having translational potential. A crucial challenge for translation into the clinics is the uncertainties of these nanoparticles in systemic toxicity and movement when being eliminated from the body. Although many reports have shown that surface-modified UCNPs does not have acute safety under *in vitro* and *in vivo* experiments along with their biodistribution, in-depth longitudinal chronic toxicity studies remain mostly elusive. Besides, the probable interactions of these nanoparticles with the immune system and the possible illicit immune response remain unexplored. Such immunological studies may shed light into the extent of biological toxicity and assess its feasibility for the ultimate translation for clinical studies. Hence, ascertaining the safety profiles of these surface-modified UCNPs needs to be systematically performed with clear objectives.

Acknowledgments

Funding

This work is supported by the Singapore Ministry of Education (Grant R143000A09133, R143000A34305), National Research Foundation, Prime Minister's Office, Singapore under its Competitive Research Program (CRP Award No. NRF-CRP15-2015-03), National Basic Research Program of China (973 Program, Grant 2015CB932200), National Natural Science Foundation of China (11774133, 21771135, 21471109, 21210001, 21701119, 21771156), CAS/SAFEA International Partnership Program for Creative Research Teams and the Early Career Scheme (ECS) fund (Grant No.: PolyU 253026/16P) from the Research Grant Council (RGC) in Hong Kong.

Notes

The authors declare no competing financial interest.

References

[1] Zhou B, Shi B, Jin D and Liu X 2015 Controlling upconversion nanocrystals for emerging applications *Nat. Nanotechnol.* **10** 924–36

[2] Wang F, Banerjee D, Liu Y, Chen X and Liu X 2010 Upconversion nanoparticles in biological labeling, imaging, and therapy *Analyst* **135** 1839–54

[3] Huang X, Han S, Huang W and Liu X 2013 Enhancing solar cell efficiency: The search for luminescent materials as spectral converters *Chem. Soc. Rev.* **42** 173–201

[4] González-Béjar M and Pérez-Prieto J 2015 Upconversion luminescent nanoparticles in physical sensing and in monitoring physical processes in biological samples *Methods Appl. Fluoresc.* **3** 042002

[5] Auzel F 2004 Upconversion and anti-stokes processes with f and d Ions in solids *Chem. Rev.* **104** 139–73

[6] Yang D, Ma P, Hou Z, Cheng Z, Li C and Lin J 2015 Current advances in lanthanide ion (Ln^{3+})-based upconversion nanomaterials for drug delivery *Chem. Soc. Rev.* **44** 1416–1448

[7] Liu X, Su L T, Karuturi S K, Luo J, Liu L, Liu X, Guo J, Sum T C, Deng R, Fan H J and Tok A I Y 2013 Photon upconversion in hetero-nanostructured photoanodes for enhanced near-infrared light harvesting *Adv. Mater.* **25** 1603–7

[8] Shang Y, Hao S, Yang C and Chen G 2015 Enhancing solar cell efficiency using photon upconversion materials *Nanomaterials* **5** 1782–809

[9] Ramasamy P, Manivasakan P and Kim J 2014 Upconversion nanophosphors for solar cell applications *RSC Adv.* **4** 34873–95

[10] Chen G, Ågren H, Ohulchanskyy T Y and Prasad P N 2015 Light upconverting core-shell nanostructures: Nanophotonic control for emerging applications *Chem. Soc. Rev.* **44** 1680–713

[11] Bettinelli M, Carlos L, Liu X 2015 Lanthanide-doped upconversion nanoparticles *Phys. Today* **68** 38–44

[12] Yang W, Li X, Chi D, Zhang H and Liu X 2014 Lanthanide-doped upconversion materials: emerging applications for photovoltaics and photocatalysis *Nanotechnology* **25** 482001

[13] Wang F and Liu X 2014 Multicolor tuning of lanthanide-doped nanoparticles by single wavelength excitation *Acc. Chem. Res.* **47** 1378–85

[14] Zhou J, Liu Q, Feng W, Sun Y and Li F 2015 Upconversion luminescent materials: Advances and applications *Chem. Rev.* **115** 395–465

[15] Tsang M-K, Bai G and Hao J 2015 Stimuli responsive upconversion luminescence nanomaterials and films for various applications *Chem. Soc. Rev.* **44** 1585–607

[16] Bai G, Tsang M K and Hao J 2015 Tuning the luminescence of phosphors: Beyond conventional chemical method *Adv. Opt. Mater.* **3** 431–62

[17] Wang G, Peng Q and Li Y 2010 Luminescence tuning of upconversion nanocrystals *Chem. - A Eur. J.* **16** 4923–31

[18] Wang F, Han Y, Lim C S, Lu Y, Wang J, Xu J, Chen H, Zhang C, Hong M and Liu X 2010 Simultaneous phase and size control of upconversion nanocrystals through lanthanide doping *Nature* **463** 1061–5

[19] Chang H, Xie J, Zhao B, Liu B, Xu S, Ren N, Xie X, Huang L and Huang W 2014 Rare earth ion-doped upconversion nanocrystals: synthesis and surface modification *Nanomaterials* **5** 1–25

[20] Chen D, Lei L, Yang A, Wang Z and Wang Y 2012 Ultra-broadband near-infrared excitable upconversion core/shell nanocrystals *Chem. Commun.* **48** 5898–900

[21] Wang J, Song H, Xu W, Dong B, Xu S, Chen B, Yu W and Zhang S 2013 Phase transition, size control and color tuning of $NaREF_4$:Yb^{3+}, Er^{3+}(RE = Y, Lu) nanocrystals *Nanoscale* **5** 3412–20

[22] Grosswhite H M and Crosswhite H 1984 Parametric model for *f*-shell configurations. I. The effective-operator Hamiltonian *J. Opt. Soc. Am. B* **1** 246–54

[23] Liu G 2014 A degenerate model of vibronic transitions for analyzing 4*f*-5*d* spectra *J. Lumin.* **152** 7–10

[24] Huang B 2016 Energy harvesting and conversion mechanisms for intrinsic upconverted mechano-persistent luminescence in CaZnOS *Phys. Chem. Chem. Phys.* **18** 25946–74

[25] Huang B 2017 The screened pseudo-charge repulsive potential in perturbed orbitals for band calculations by DFT+U *Phys. Chem. Chem. Phys.* **19** 8008–25

[26] Han S, Deng R, Xie X and Liu X 2014 Enhancing luminescence in lanthanide-doped upconversion nanoparticles *Angew. Chem. Int. Ed.* **53** 11702–15

[27] Wang F, Deng R, Wang J, Wang Q, Han Y, Zhu H, Chen X and Liu X 2011 Tuning upconversion through energy migration in core-shell nanoparticles *Nat. Mater.* **10** 968–73

[28] Huang B 2016 4*f* fine-structure levels as the dominant error in the electronic structures of binary lanthanide oxides *J. Comput. Chem.* **37** 825–35

[29] Liu G and Jacquier B 2005 *Spectroscopic Properties of Rare Earths in Optical Materials* vol 83

[30] Dieke G H, Crosswhite H M and Dunn B 1961 Emission spectra of the doubly and triply ionized rare earths *J. Opt. Soc. Am.* **51** 820-827

[31] Qin X, Liu X, Huang W, Bettinelli M and Liu X 2017 Lanthanide-activated phosphors based on 4*f*-5*d* optical transitions: theoretical and experimental Aspects *Chem. Rev.* **117** 4488–527

[32] Dong H, Sun L-D and Yan C-H 2013 Basic understanding of the lanthanide related upconversion emissions *Nanoscale* **5** 5703-14

[33] Su Q, Han S, Xie X, Zhu H, Chen H, Chen C K, Liu R S, Chen X, Wang F and Liu X 2012 The effect of surface coating on energy migration-mediated upconversion *J. Am. Chem. Soc.* **134** 20849–57

[34] Bünzli J-C G and Piguet C 2005 Taking advantage of luminescent lanthanide ions *Chem. Soc. Rev.* **34** 1048-77

[35] Yan C, Zhao H, Perepichka D F and Rosei F 2016 Lanthanide ion doped upconverting nanoparticles: synthesis, structure and properties *Small* 3888–907

[36] Dong H, Sun L D and Yan C H 2013 Basic understanding of the lanthanide related upconversion emissions *Nanoscale* **5** 5703–14

[37] Huang B, Dong H, Wong K L, Sun L D and Yan C H 2016 Fundamental view of electronic structures of β-$NaYF_4$, β-$NaGdF_4$, and β-$NaLuF_4$ *J. Phys. Chem. C* **120** 18858–70

[38] Huang B, Dong H, Wong K-L, Sun L and Yan C 2017 Interface formation energy, bonding, energy band alignment in α-$NaYF_4$ related core shell models: for future multi-layer core shell luminescence materials *J. Rare Earths* **35** 315–34

[39] Zhao J, Jin D, Schartner E P, Lu Y, Liu Y, Zvyagin A V., Zhang L, Dawes J M, Xi P, Piper J A, Goldys E M and Monro T M 2013 Single-nanocrystal sensitivity achieved by enhanced upconversion luminescence *Nat. Nanotechnol.* **8** 729–34

[40] Dong H, Sun L D, Feng W, Gu Y, Li F and Yan C H 2017 Versatile spectral and lifetime multiplexing nanoplatform with excitation orthogonalized upconversion luminescence *ACS Nano* **11** 3289–97

[41] Han S, Qin X, An Z, Zhu Y, Liang L, Han Y, Huang W and Liu X 2016 Multicolour synthesis in lanthanide-doped nanocrystals through cation exchange in water *Nat. Commun.* **7** 1–7

[42] Wang H, Lu W, Yi Z, Rao L, Zeng S and Li Z 2015 Enhanced upconversion luminescence and single-band red emission of $NaErF_4$nanocrystals *via* Mn^{2+} doping *J. Alloys Compd.* **618** 776–80

[43] Tian G, Gu Z, Zhou L, Yin W, Liu X, Yan L, Jin S, Ren W, Xing G, Li S and Zhao Y 2012 Mn^{2+} dopant-controlled synthesis of $NaYF_4$:Yb/Er upconversion nanoparticles for in vivo imaging and drug delivery *Adv. Mater.* **24** 1226–31

[44] Xie X, Gao N, Deng R, Sun Q, Xu Q H and Liu X 2013

Mechanistic investigation of photon upconversion in Nd^{3+}-sensitized core-shell nanoparticles *J. Am. Chem. Soc.* **135** 12608–11

[45] Chen D, Lei L, Zhang R, Yang A, Xu J and Wang Y 2012 Intrinsic single-band upconversion emission in colloidal Yb/Er(Tm):$Na_3Zr(Hf)F_7$nanocrystals *Chem. Commun.* **48** 10630–2

[46] Chen D and Wang Y 2013 Impurity doping: A novel strategy for controllable synthesis of functional lanthanide nanomaterials *Nanoscale* **5** 4621–37

[47] Wang F and Liu X 2008 Upconversion multicolor fine-tuning: Visible to near-infrared emission from lanthanide-doped $NaYF_4$ nanoparticles *J. Am. Chem. Soc.* **130** 5642–3

[48] Mai H X, Zhang Y W, Sun L D and Yan C H 2007 Highly efficient multicolor up-conversion emissions and their mechanisms of monodisperse $NaYF_4$:Yb,Er core and core/shell-structured nanocrystals *J. Phys. Chem. C* **111** 13721–9

[49] Yin A, Zhang Y, Sun L and Yan C 2010 Colloidal synthesis and blue based multicolor upconversion emissions of size and composition controlled monodisperse hexagonal $NaYF_4$:Yb,Tm nanocrystals *Nanoscale* **2** 953–9

[50] Shen J, Chen G, Ohulchanskyy T Y, Kesseli S J, Buchholz S, Li Z, Prasad P N and Han G 2013 Tunable near infrared to ultraviolet upconversion luminescence enhancement in (α-$NaYF_4$:Yb,Tm)/CaF_2 core/shell nanoparticles for in situ real-time recorded biocompatible photoactivation *Small* **9** 3213–7

[51] Zhai X, Liu S, Zhang Y, Qin G and Qin W 2014 Controlled synthesis of ultrasmall hexagonal $NaTm_{0.02}Lu_{0.98-x}Yb_xF_4$ nanocrystals with enhanced upconversion luminescence *J. Mater. Chem. C* **2** 2037–44

[52] Qiu H, Chen G, Fan R, Yang L, Liu C, Hao S, Sailor M J, Ågren H, Yang C and Prasad P N 2014 Intense ultraviolet upconversion emission from water-dispersed colloidal YF_3:Yb^{3+}/Tm^{3+} rhombic nanodisks *Nanoscale* **6** 753–7

[53] Lu Y, Zhao J, Zhang R, Liu Y, Liu D, Goldys E M, Yang X, Xi P, Sunna A, Lu J, Shi Y, Leif R C, Huo Y, Shen J, Piper J A, Robinson J P and Jin D 2014 Tunable lifetime multiplexing using luminescent nanocrystals *Nat. Photonics* **8** 32–6

[54] Huang B, Sun M, Dougherty A W, Dong H, Xu Y-J, Sun L-D and Yan C-H 2017 Unravelling the energy transfer of Er^{3+}-self-sensitized upconversion in Er^{3+}-Yb^{3+}-Er^{3+} clustered core@shell nanoparticles *Nanoscale* **9** 18490-97

[55] Bai Y, Wang Y, Yang K, Zhang X, Peng G, Song Y, Pan Z and Wang C H 2008 The effect of Li on the spectrum of Er^{3+} in Li- and Er-codoped ZnO nanocrystals *J. Phys. Chem. C* **112** 12259–63

[56] Yin W, Zhao L, Zhou L, Gu Z, Liu X, Tian G, Jin S, Yan L, Ren W, Xing G and Zhao Y 2012 Enhanced red emission from GdF_3:Yb^{3+},Er^{3+} upconversion nanocrystals by Li^+ doping and their application for bioimaging *Chem.- A Eur. J.* **18** 9239–45

[57] Chen G, Liu H, Liang H, Somesfalean G and Zhang Z 2008 Upconversion emission enhancement in Yb^{3+}/Er^{3+}-Codoped Y_2O_3 nanocrystals by tridoping with Li^+ Ions *J. Phys. Chem. C* **112** 12030–6

[58] Liang H, Chen G, Liu H and Zhang Z 2009 Ultraviolet upconversion luminescence enhancement in Yb^{3+}/Er^{3+}-codoped Y_2O_3 nanocrystals induced by tridoping with Li^+ ions *J. Lumin.* **129** 197–202

[59] Jiang L, Xiao S, Yang X, Ding J and Dong K 2012 Enhancement of up-conversion luminescence in Zn_2SiO_4:Yb^{3+},Er^{3+} by co-doping with Li^+or Bi^{3+} *Appl. Phys. B Lasers Opt.* **107** 477–481

[60] Ramasamy P, Chandra P, Rhee S W and Kim J 2013 Enhanced upconversion luminescence in $NaGdF_4$:Yb,Er nanocrystals by Fe^{3+} doping and their application in bioimaging *Nanoscale* **5** 8711–7

[61] Wang J, Deng R, Macdonald M A, Chen B, Yuan J, Wang F, Chi D, Andy Hor T S, Zhang P, Liu G, Han Y and Liu X 2014 Enhancing multiphoton upconversion through energy clustering at sublattice level *Nat. Mater.* **13** 157–62

[62] Wang L, Li X, Li Z, Chu W, Li R, Lin K, Qian H, Wang Y, Wu C, Li J, Tu D, Zhang Q, Song L, Jiang J, Chen X, Luo Y, Xie Y and Xiong Y 2015 A new cubic phase for a $NaYF_4$ host matrix offering high upconversion luminescence efficiency *Adv. Mater.* **27** 5528–33

[63] Chen G, Qiu H, Fan R, Hao S, Tan S, Yang C and Han G 2012 Lanthanide-doped ultrasmall yttrium fluoride nanoparticles with enhanced multicolor upconversion photoluminescence *J. Mater. Chem.* **22** 20190–6

[64] Dorenbos P 2005 Valence stability of lanthanide ions in inorganic compounds *Chem. Mater.* **17** 6452–6

[65] Dorenbos P 2004 Locating lanthanide impurity levels in the forbidden band of host crystals *J. Lumin.* **108** 301–5

[66] Zhang Y, Lin J D, Vijayaragavan V, Bhakoo K K and Tan T T Y 2012 Tuning sub-10 nm single-phase NaMnF3nanocrystals as ultrasensitive hosts for pure intense fluorescence and excellent T_1 magnetic resonance imaging *Chem. Commun.* **48** 10322–4

[67] Huang Z, Yi M, Gao H, Zhang Z and Mao Y 2017 Enhancing single red band upconversion luminescence of $KMnF_3$:Yb^{3+}/Er^{3+} nanocrystals by Mg^{2+} doping *J. Alloys Compd.* **694** 241–5

[68] Wang J, Wang F, Wang C, Liu Z and Liu X 2011 Single-band upconversion emission in lanthanide-doped $KMnF_3$ nanocrystals *Angew. Chem. Int. Ed.* **50** 10369–72

[69] Patra A, Friend C S, Kapoor R and Prasad P N 2003 Effect of crystal nature on upconversion luminescence in Er^{3+}:ZrO_2 nanocrystals *Appl. Phys. Lett.* **83** 284–6

[70] Vetrone F, Boyer J C, Capobianco J A, Speghini A and Bettinelli M 2002 NIR to visible upconversion in nanocrystalline and bulk Lu_2O_3:Er^{3+} *J. Phys. Chem. B* **106** 5622–8

[71] Zeng J H, Xie T, Li Z H and Li Y 2007 Monodispersed nanocrystalline fluoroperovskite up-conversion phosphors *Cryst. Growth Des.* **7** 2774–7

[72] Chen X, Jin L, Kong W, Sun T, Zhang W, Liu X, Fan J, Yu S F and Wang F 2016 Confining energy migration in upconversion nanoparticles towards deep ultraviolet lasing *Nat. Commun.* **7** 1–6

[73] Zhao J, Lu Z, Yin Y, McRae C, Piper J A, Dawes J M, Jin D and Goldys E M 2013 Upconversion luminescence with tunable lifetime in $NaYF_4$:Yb,Er nanocrystals: Role of nanocrystal size *Nanoscale* **5** 944–52

[74] Michalet X, Pinaud F F, Bentolila L A, Tsay J M, Doose S, Li J J, Sundaresan G, Wu A M, Gambhir S S and Weiss S 2005 Quantum dots for live cells, in vivo imaging, and diagnostics *Science* **307** 538–44

[75] Xue X, Uechi S, Tiwari R N, Duan Z, Liao M, Yoshimura M, Suzuki T and Ohishi Y 2013 Size-dependent upconversion luminescence and quenching mechanism of $LiYF_4$:Er^{3+}/Yb^{3+} nanocrystals with oleate ligand adsorbed *Opt. Mater. Express* **3** 989-99

[76] Wang F, Wang J and Liu X 2010 Direct evidence of a surface quenching effect on size-dependent luminescence of

upconversion nanoparticles *Angew. Chem. Int. Ed.* **49** 7456–60

[77] Huang B 2015 Native point defects in CaS: Focus on intrinsic defects and rare earth ion dopant levels for up-converted persistent luminescence *Inorg. Chem.* **54** 11423–40

[78] Zhou B, Yang W, Han S, Sun Q and Liu X 2015 Photon upconversion through Tb^{3+}-mediated interfacial energy transfer *Adv. Mater.* **27** 6208–12

[79] Zhou B, Tao L, Chai Y, Lau S P, Zhang Q and Tsang Y H 2016 Constructing interfacial energy transfer for photon up- and down-conversion from lanthanides in a core–shell nanostructure *Angew. Chem. Int. Ed.* **55** 12356–60

[80] Huang P, Zheng W, Zhou S, Tu D, Chen Z, Zhu H, Li R, Ma E, Huang M and Chen X 2014 Lanthanide-doped $LiLuF_4$ upconversion nanoprobes for the detection of disease biomarkers. *Angew. Chem. Int. Ed.* **53** 1252–7

[81] Kumar R, Nyk M, Ohulchanskyy T Y, Flask C a and Prasad P N 2009 Combined optical and MR bioimaging using rare earth ion doped $NaYF_4$ nanocrystals *Adv. Funct. Mater.* **19** 853–9

[82] Bogdan N, Vetrone F, Ozin G A and Capobianco J A 2011 Synthesis of ligand-free colloidally stable water dispersible brightly luminescent lanthanide-doped upconverting nanoparticles *Nano Lett.* **11** 835–40

[83] Zou W, Visser C, Maduro J A, Pshenichnikov M S and Hummelen J C 2012 Broadband dye-sensitized upconversion of near-infrared light *Nat. Photonics* **6** 560–4

[84] Zhang C, Ou H P, Liao L Y, Feng W, Sun W, Li Z X, Xu C H, Fang C J, Sun L D, Zhang Y W and Yan C H 2010 Luminescence modulation of ordered upconversion nanopatterns by a photochromic diarylethene: Rewritable optical storage with nondestructive readout *Adv. Mater.* **22** 633–7

[85] Yi G and Chow G-M 2007 Water-Soluble $NaYF_4$:Yb,Er(Tm)/$NaYF_4$/Polymer core/shell/shell nanoparticles with significant enhancement of upconversion fluorescence *Chem. Mater.* **19** 341–3

[86] Li Z and Zhang Y 2006 Monodisperse silica-coated polyvinyl-pyrrolidone/$NaYF_4$ nanocrystals with multicolor upconversion fluorescence emission *Angew. Chem. Int. Ed.* **45** 7732–5

[87] Yan C, Dadvand A, Rosei F and Perepichka D F 2010 Near-IR photoresponse in new up-converting CdSe/$NaYF_4$:Yb,Er nanoheterostructures *J. Am. Chem. Soc.* **132** 8868–9

[88] Xu B, Zhang X, Huang W, Yang Y, Ma Y, Gu Z, Zhai T and Zhao Y 2016 Nd^{3+} sensitized dumbbell-like upconversion nanoparticles for photodynamic therapy application *J. Mater. Chem. B* **4** 2776–84

[89] Wang Y F, Liu G Y, Sun L D, Xiao J W, Zhou J C and Yan C H 2013 Nd^{3+}-sensitized upconversion nanophosphors: Efficient in vivo bioimaging probes with minimized heating effect *ACS Nano* **7** 7200–6

[90] Xie X, Li Z, Zhang Y, Guo S, Pendharkar A I, Lu M, Huang L, Huang W and Han G 2017 Emerging ≈800 nm Excited Lanthanide-Doped Upconversion Nanoparticles *Small* **13** 1602843

[91] Zhan Q, Qian J, Liang H, Somesfalean G, Wang D, He S, Zhang Z and Andersson-Engels S 2011 Using 915 nm laser excited Tm^{3+}/Er^{3+}/Ho^{3+}-doped $NaYbF_4$ upconversion nanoparticles for in vitro and deeper in vivo bioimaging without overheating irradiation *ACS Nano* **5** 3744–57

[92] Mi Z, Zhang Y, Vanga S K, Chen C B, Tan H Q, Watt F, Liu X and Bettiol A A 2015 Subwavelength imaging through ion-beam-induced upconversion *Nat. Commun.* **6** 8832

[93] Deng R, Qin F, Chen R, Huang W, Hong M and Liu X 2015 Temporal full-colour tuning through non-steady-state upconversion *Nat. Nanotechnol.* **10** 237–42

[94] Zhang C, Yang L, Zhao J, Liu B, Han M Y and Zhang Z 2015 White-light emission from an integrated upconversion nanostructure: Toward multicolor displays modulated by laser power *Angew. Chem. Int. Ed.* **54** 11531–5

[95] Liu Y, Lu Y, Yang X, Zheng X, Wen S, Wang F, Vidal X, Zhao J, Liu D, Zhou Z, Ma C, Zhou J, Piper J A, Xi P and Jin D 2017 Amplified stimulated emission in upconversion nanoparticles for super-resolution nanoscopy *Nature* **543** 229–33

[96] Shin K, Jung T, Lee E, Lee G, Goh Y, Heo J, Jung M, Jo E-J, Lee H, Kim M-G and Lee K T 2017 Distinct mechanisms for the upconversion of $NaYF_4$:Yb^{3+},Er^{3+} nanoparticles revealed by stimulated emission depletion *Phys. Chem. Chem. Phys.* **19** 9739–44

[97] Zhan Q, Liu H, Wang B, Wu Q, Pu R, Zhou C, Huang B, Peng X, Ågren H and He S 2017 Achieving high-efficiency emission depletion nanoscopy by employing cross relaxation in upconversion nanoparticles *Nat. Commun.* **8** 1058

[98] Carnall W T, Goodman G L, Rana R S, Vandevelde P, Fluyt L and GÖrller-Walrand C 1986 Crystal-field analysis of Ho^{3+} LaF_3 and Er^{3+} LaF_3 in C_{2v} site symmetry *J. Less-Common Met.* **116** 17-29

[99] Carnall W T, Goodman G L, Rajnak K and Rana R S 1989 A systematic analysis of the spectra of the lanthanides doped into single crystal LaF_3 *J. Chem. Phys.* **90** 3443–57

[100] Liu G K, Zhuang H Z and Chen X Y 2002 Restricted phonon relaxation and anomalous thermalization of rare earth ions in nanocrystals *Nano Lett.* **2** 535–9

[101] Auzel F 2005 Up-conversion in Re-doped solids *Spectroscopic Properties of Rare Earths in Optical Materials* **83** 266–319

[102] Yang D, Ma P, Hou Z, Cheng Z, Li C and Lin J 2015 Current advances in lanthanide ion (Ln^{3+})-based upconversion nanomaterials for drug delivery *Chem. Soc. Rev.* **44** 1416–48

[103] Liz-Marzán L M, Murphy C J and Wang J 2014 Nanoplasmonics *Chem. Soc. Rev.* **43** 3820–2

[104] Linic S, Christopher P and Ingram D B 2011 Plasmonic-metal nanostructures for efficient conversion of solar to chemical energy *Nat. Mater.* **10** 911–21

[105] Jain P K and El-Sayed M A 2010 Plasmonic coupling in noble metal nanostructures *Chem. Phys. Lett.* **487** 153–64

[106] Schuller J A, Barnard E S, Cai W, Jun Y C, White J S and Brongersma M L 2010 Plasmonics for extreme light concentration and manipulation *Nat. Mater.* **9** 193–204

[107] Buffman D R, Matter B, Of O P, Bohren C F, Huffman D R M R, Stevens W L, Silvonen K, Purcell E M, Rev A, Astrophys A, Of O P, Modes S, Matter B, Matrix S, Huffman D R M R, Buffman D R, Bohren C F, Huffman D R M R, Buffman D R, Bohren C F, Huffman D R M R, Buffman D R, Purcell E M, Rev A, Astrophys A, Buffman D R, Silvonen K, Bohren C F, Huffman D R M R, Of F, Mie G, Bohren C F, Huffman D R M R, Matrix S and Stevens W L 2007 *Absorption and Scattering of Light by Small Particles* **38**

[108] Xu W, Chen X and Song H 2017 Upconversion manipulation by local electromagnetic field *Nano Today* **17** 54–78

[109] Liu X and Lei D Y 2015 Simultaneous excitation and emission enhancements in upconversion luminescence using plasmonic double-resonant gold nanorods *Sci. Rep.* **5** 15235

[110] Zhang W, Ding F and Chou S Y 2012 Large enhancement of upconversion luminescence of $NaYF_4:Yb^{3+}/Er^{3+}$ Nanocrystal by 3D plasmonic nano-antennas *Adv. Mater.* **24** OP236-OP241

[111] Wang Y L, Estakhri N M, Johnson A, Li H Y, Xu L X, Zhang Z, Alù A, Wang Q Q and Shih C K 2015 Tailoring plasmonic enhanced upconversion in single $NaYF_4$: Yb^{3+}/Er^{3+} nanocrystals *Sci. Rep.* **5** 10196

[112] Park W, Lu D and Ahn S 2015 Plasmon enhancement of luminescence upconversion *Chem. Soc. Rev.*

[113] Lakowicz J R 2001 Radiative decay engineering: Biophysical and biomedical applications *Anal. Biochem.* **298** 1–24

[114] Wu D M, García-Etxarri A, Salleo A and Dionne J A 2014 Plasmon-enhanced upconversion *J. Phys. Chem. Lett.* **5** 4020–31

[115] Feng W, Sun L D and Yan C H 2009 Ag nanowires enhanced upconversion emission of $NaYF_4$:Yb,Er nanocrystals *via* a direct assembly method *Chem. Commun.* 4393–5

[116] Schietinger S, Aichele T, Wang H Q, Nann T and Benson O 2010 Plasmon-enhanced upconversion in single $NaYF_4:Yb^{3+}/Er^{3+}$ codoped nanocrystals *Nano Lett.* **10** 134–8

[117] Greybush N J, Saboktakin M, Ye X, Della Giovampaola C, Oh S J, Berry N E, Engheta N, Murray C B and Kagan C R 2014 Plasmon-enhanced upconversion luminescence in single nanophosphor-nanorod heterodimers formed through template-assisted self-assembly *ACS Nano* **8** 9482–91

[118] He J, Zheng W, Ligmajer F, Chan C, Bao Z, Wong K, Chen X, Hao J, Dai J, Yu S and Lei D Y 2017 Plasmonic enhancement and polarization dependence of nonlinear upconversion emissions from single gold satellite nanostructures *Light Sci. Appl.* **6** e16217

[119] Mauser N, Piatkowski D, Mancabelli T, Nyk M, Mackowski S and Hartschuh A 2015 Tip enhancement of upconversion photoluminescence from rare earth ion doped nanocrystals *ACS Nano* **9** 3617–26

[120] Xu W, Song H, Chen X, Wang H, Cui S, Zhou D, Zhou P and Xu S 2015 Upconversion luminescence enhancement of Yb^{3+},Nd^{3+} sensitized $NaYF_4$ core–shell nanocrystals on Ag grating films *Chem. Commun.* **51** 1502–5

[121] Saboktakin M, Ye X, Chettiar U K, Engheta N, Murray C B and Kagan C R 2013 Plasmonic enhancement of nanophosphor upconversion luminescence in Au nanohole arrays *ACS Nano* **7** 7186–92

[122] Sun Q C, Mundoor H, Ribot J C, Singh V, Smalyukh I I and Nagpal P 2014 Plasmon-enhanced energy transfer for improved upconversion of infrared radiation in doped-lanthanide nanocrystals *Nano Lett.* **14** 101–6

[123] Fisher J, Zhao B, Lin C, Berry M, May P S and Smith S 2015 Spectroscopic Imaging and Power Dependence of Near-Infrared to Visible Upconversion Luminescence from $NaYF_4:Yb^{3+},Er^{3+}$ Nanoparticles on Nanocavity Arrays *J. Phys. Chem. C* **119** 24976–82

[124] Saboktakin M, Ye X, Oh S J, Hong S H, Fafarman A T, Chettiar U K, Engheta N, Murray C B and Kagan C R 2012 Metal-enhanced upconversion luminescence tunable through metal nanoparticle-nanophosphor separation *ACS Nano* **6** 8758–66

[125] Yuan P, Lee Y H, Gnanasammandhan M K, Guan Z, Zhang Y and Xu Q-H 2012 Plasmon enhanced upconversion luminescence of $NaYF_4$:Yb,Er@SiO_2@Ag core–shell nanocomposites for cell imaging *Nanoscale* **4** 5132-7

[126] Bang D, Jo E J, Hong S, Byun J Y, Lee J Y, Kim M G and Lee L P 2017 Asymmetric Nanocrescent Antenna on Upconversion Nanocrystal *Nano Lett.* **17** 6583–90

[127] Hao J, Zhang Y and Wei X 2011 Electric-induced enhancement and modulation of upconversion photoluminescence in epitaxial $BaTiO_3$:Yb/Er thin films *Angew. Chem. Int. Ed.* **50** 6876–80

[128] Wang Z, Senden T and Meijerink A 2017 Photonic effects for magnetic dipole transitions *J. Phys. Chem. Lett.* **8** 5689–94

[129] Liu Y, Wang D, Shi J, Peng Q and Li Y 2013 Magnetic tuning of upconversion luminescence in lanthanide-doped bifunctional nanocrystals *Angew. Chem. Int. Ed.* **52** 4366–9

[130] Xiao Q, Zhang Y, Zhang H, Dong G, Han J and Qiu J 2016 Dynamically tuning the up-conversion luminescence of Er^{3+}/Yb^{3+} co-doped sodium niobate nano-crystals through magnetic field *Sci. Rep.* **6** 1–9

[131] Li Z X, Li L Le, Zhou H P, Yuan Q, Chen C, Sun L D and Yan C H 2009 Colour modification action of an upconversion photonic crystal *Chem. Commun.* 6616–8

[132] Yin Z, Li H, Xu W, Cui S, Zhou D, Chen X, Zhu Y, Qin G and Song H 2016 Local field modulation induced three-order upconversion enhancement: Combining surface plasmon effect and photonic crystal effect *Adv. Mater.* **28** 2518–25

[133] Gan X, Yao X, Shiue R-J, Hatami F and Englund D 2015 Photonic crystal cavity-assisted upconversion infrared photodetector *Opt. Express* **23** 12998-13004

[134] Marques-Hueso J, Peretti R, Abargues R, Richards B S, Seassal C and Martínez-Pastor J P 2015 Photonic crystal-driven spectral concentration for upconversion photovoltaics *Adv. Opt. Mater.* **3** 568–74

[135] Yang Z, Yan D, Zhu K, Song Z, Yu X, Zhou D, Yin Z and Qiu J 2012 Modification of the upconversion spontaneous emission in photonic crystals *Mater. Chem. Phys.* **133** 584–7

[136] Niu W, Su L T, Chen R, Chen H, Wang Y, Palaniappan A, Sun H and Yoong Tok A I 2014 3-Dimensional photonic crystal surface enhanced upconversion emission for improved near-infrared photoresponse *Nanoscale* **6** 817–24

[137] Yin Z, Zhu Y, Xu W, Wang J, Xu S, Dong B, Xu L, Zhang S and Song H 2013 Remarkable enhancement of upconversion fluorescence and confocal imaging of PMMA Opal/$NaYF_4:Yb^{3+}$, Tm^{3+}/Er^{3+} nanocrystals *Chem. Commun.* **49** 3781–3

[138] Zhang S Z, Sun L D, Tian H, Liu Y, Wang J F and Yan C H 2009 Reversible luminescence switching of $NaYF_4$:Yb,Er nanoparticles with controlled assembly of gold nanoparticles *Chem. Commun.* 2547–9.

[139] Sun L N, Peng H, Stich M I J, Achatz D and Wolfbeis O S 2009 PH sensor based on upconverting luminescent lanthanide nanorods *Chem. Commun.* 5000–2

[140] Tvingstedt K, Dal Zilio S, Inganäs O and Tormen M 2008 Trapping light with micro lenses in thin film organic photovoltaic cells *Opt. Express* **16** 21608-15

[141] Cho C and Lee J-Y 2013 Multi-scale and angular analysis of ray-optical light trapping schemes in thin-film solar cells: Micro lens array, V-shaped configuration, and double parabolic trapper *Opt. Express* **21** A276-A284

[142] Peer A, Biswas R, Park J-M, Shinar R and Shinar J 2017

Light management in perovskite solar cells and organic LEDs with microlens arrays *Opt. Express* **25** 10704-09

[143] Lin H Y, Ho Y H, Lee J H, Chen K Y, Fang J H, Hsu S C, Wei M K, Lin H Y, Tsai J H and Wu T C 2008 Patterned microlens array for efficiency improvement of small-pixelated organic light-emitting devices. *Opt. Express* **16** 11044–51

[144] Wrzesniewski E, Eom S H, Cao W, Hammond W T, Lee S, Douglas E P and Xue J 2012 Enhancing light extraction in top-emitting organic light-emitting devices using molded transparent polymer microlens arrays *Small* **8** 2647–51

[145] Li Y, Liu X, Yang X, Lei H, Zhang Y and Li B 2017 Enhancing upconversion fluorescence with a natural bio-microlens *ACS Nano* **11** 10672–80

[146] Brites C D S, Xie X, Debasu M L, Qin X, Chen R, Huang W, Rocha J, Liu X and Carlos L D 2016 Instantaneous ballistic velocity of suspended Brownian nanocrystals measured by upconversion nanothermometry *Nat. Nanotechnol.* **11** 851–6

[147] Geitenbeek R G, Prins P T, Albrecht W, Van Blaaderen A, Weckhuysen B M and Meijerink A 2017 $NaYF_4$:Er^{3+},Yb^{3+}/SiO_2 core/shell upconverting nanocrystals for luminescence thermometry up to 900 K *J. Phys. Chem. C* **121** 3503–10

[148] Fischer L H, Harms G S and Wolfbeis O S 2011 Upconverting nanoparticles for nanoscale thermometry *Angew. Chem. Int. Ed.* **50** 4546–51

[149] Yu W, Xu W, Song H and Zhang S 2014 Temperature-dependent upconversion luminescence and dynamics of $NaYF_4$:Yb^{3+}/Er^{3+} nanocrystals: influence of particle size and crystalline phase *Dalt. Trans.* **43** 6139–47

[150] Zhou J, Wen S, Liao J, Clarke C, Tawfik S A, Ren W, Mi C, Wang F and Jin D 2018 Activation of the surface dark-layer to enhance upconversion in a thermal field *Nat. Photonics* **12** 154–8

[151] Wang J, Ming T, Jin Z, Wang J, Sun L D and Yan C H 2014 Photon energy upconversion through thermal radiation with the power efficiency reaching 16% *Nat. Commun.* **5** 5669

[152] Dou Q and Zhang Y 2011 Tuning of the structure and emission spectra of upconversion nanocrystals by alkali ion doping *Langmuir* **27** 13236–41

[153] Wisser M D, Chea M, Lin Y, Wu D M, Mao W L, Salleo A and Dionne J A 2015 Strain-induced modification of optical selection rules in lanthanide-based upconverting nanoparticles *Nano Lett.* **15** 1891–7

[154] Lay A, Wang D S, Wisser M D, Mehlenbacher R D, Lin Y, Goodman M B, Mao W L and Dionne J A 2017 Upconverting nanoparticles as optical sensors of nano- to micro-newton forces *Nano Lett.* **17** 4172–7

[155] Zhang H, Peng D, Wang W, Dong L and Pan C 2015 Mechanically induced light emission and infrared-laser-induced upconversion in the Er-doped CaZnOS multifunctional piezoelectric semiconductor for optical pressure and temperature sensing *J. Phys. Chem. C* **119** 28136–42

[156] Li L, Wondraczek L, Li L, Zhang Y, Zhu Y, Peng M and Mao C 2018 CaZnOS:Nd^{3+} emits tissue-penetrating near-infrared light upon force loading *ACS Appl. Mater. Interfaces* **10** 14509–16

[157] Ting T C T 1992 *Anisotropic Elasticity: Theory and Applications*

[158] Hermannstädter C, Witzany M, Heldmaier M, Hafenbrak R, Jöns K D, Beirne G J and Michler P 2012 Polarization anisotropic luminescence of tunable single lateral quantum dot molecules *J. Appl. Phys.* **111** 063526

[159] Zhou J, Chen G, Wu E, Bi G, Wu B, Teng Y, Zhou S and Qiu J 2013 Ultrasensitive polarized up-conversion of Tm^{3+}–Yb^{3+} doped β-$NaYF_4$ single nanorod *Nano Lett.* **13** 2241–6

[160] Chen P, Song M, Wu E, Wu B, Zhou J, Zeng H, Liu X and Qiu J 2015 Polarization modulated upconversion luminescence: Single particle vs. few-particle aggregates *Nanoscale* **7** 6462–6

[161] Gong S, Ren Z, Jiang S, Li M, Li X, Wei X, Xu G, Shen G and Han G 2014 Phase-modified up-conversion luminescence in Er-doped single-crystal $PbTiO_3$ nanofibers *J. Phys. Chem. C* **118** 5486–93

[162] Ostrowski A D, Chan E M, Gargas D J, Katz E M, Han G, Schuck P J, Milliron D J and Cohen B E 2012 Controlled synthesis and single-particle imaging of bright, sub-10 nm lanthanide-doped upconverting nanocrystals *ACS Nano* **6** 2686–92

[163] Chan E M, Han G, Goldberg J D, Gargas D J, Ostrowski A D, Schuck P J, Cohen B E and Milliron D J 2012 Combinatorial discovery of lanthanide-doped nanocrystals with spectrally pure upconverted emission *Nano Lett.* **12** 3839–45

[164] Hazarika P and Russell D A 2012 Advances in fingerprint analysis *Angew. Chem. Int. Ed.* **51** 3524–31

[165] Wang J, Wei T, Li X, Zhang B, Wang J, Huang C and Yuan Q 2014 Near-infrared-light-mediated imaging of latent fingerprints based on molecular recognition *Angew. Chem. Int. Ed.* **53** 1616–20

[166] Sukul P P, Kumar K 2018 Photoluminescence study of Yb^{3+}/Er^{3+} co-doped Sb_2O_3-WO_3-Li_2O (SWL) ceramic phosphor for fingerprint detection in forensic science and security writing *Optical Materials and Biomaterials in Security and Defence Systems Technology XV*. *International Society for Optics and Photonics*, 10801: 108010E.

[167] Zhang Y, Zhang L, Deng R, Tian J, Zong Y, Jin D and Liu X 2014 Multicolor barcoding in a single upconversion crystal *J. Am. Chem. Soc.* **136** 4893–6

[168] Lee J, Bisso P W, Srinivas R L, Kim J J, Swiston A J and Doyle P S 2014 Universal process-inert encoding architecture for polymer microparticles *Nat. Mater.* **13** 524–9

[169] Meruga J M, Baride A, Cross W, Kellar J J and May P S 2014 Red-green-blue printing using luminescence-upconversion inks *J. Mater. Chem. C* **2** 2221–7

[170] Chen X, Xu W, Zhang L, Bai X, Cui S, Zhou D, Yin Z, Song H and Kim D H 2015 Large Upconversion Enhancement in the "islands" Au-Ag Alloy/$NaYF_4$:Tm^{3+}/ Yb^{3+}, Tm^{3+}/Er^{3+} Composite Films, and Fingerprint Identification *Adv. Funct. Mater.* **25** 5462–71

[171] Li J, Zhu X, Xue M, Feng W, Ma R and Li F 2016 Nd^{3+}-sensitized upconversion nanostructure as a dual-channel emitting optical probe for near infrared-to-near infrared fingerprint imaging *Inorg. Chem.* **55** 10278–83

[172] Zhou D, Liu D, Xu W, Chen X, Yin Z, Bai X, Dong B, Xu L and Song H 2017 Synergistic upconversion enhancement induced by multiple physical effects and an angle-dependent anticounterfeit application *Chem. Mater.* **29** 6799–809

[173] Gupta B K, Haranath D, Saini S, Singh V N and Shanker V 2010 Synthesis and characterization of ultra-fine Y_2O_3:Eu^{3+}nanophosphors for luminescent security ink applications *Nanotechnology* **21** 055607

[174] Kumar P, Dwivedi J and Gupta B K 2014 Highly luminescent dual mode rare-earth nanorod assisted multi-stage excitable security ink for anti-counterfeiting

applications *J. Mater. Chem. C* **2** 10468–75

[175] Chen B, Kong W, Liu Y, Lu Y, Li M, Qiao X, Fan X and Wang F 2017 Crystalline hollow microrods for site-selective enhancement of nonlinear photoluminescence *Angew. Chem. Int. Ed.* **56** 10383–7

[176] Liu X, Wang Y, Li X, Yi Z, Deng R, Liang L, Xie X, Loong D T B, Song S, Fan Di, All A H, Zhang H, Huang L and Liu X 2017 Binary temporal upconversion codes of Mn^{2+}-activated nanoparticles for multilevel anti-counterfeiting *Nat. Commun.* **8** 899

[177] Su Q, Feng W, Yang D and Li F 2017 Resonance energy transfer in upconversion nanoplatforms for selective biodetection *Acc. Chem. Res.* **50** 32–40

[178] Chen Z, Chen H, Hu H, Yu M, Li F, Zhang Q, Zhou Z, Yi T and Huang C 2008 Versatile synthesis strategy for carboxylic acid-functionalized upconverting nanophosphors as biological labels *J. Am. Chem. Soc.* **130** 3023–9

[179] Liu Q, Peng J, Sun L and Li F 2011 High-efficiency upconversion luminescent sensing and bioimaging of Hg(II) by chromophoric ruthenium complex-assembled nanophosphors *ACS Nano* **5** 8040–8

[180] Zou X, Liu Y, Zhu X, Chen M, Yao L, Feng W and Li F 2015 An Nd^{3+}-sensitized upconversion nanophosphor modified with a cyanine dye for the ratiometric upconversion luminescence bioimaging of hypochlorite *Nanoscale* **7** 4105–13

[181] Smolyaninov I I, Elliott J, Zayats A V. and Davis C C 2005 Far-field optical microscopy with a nanometer-scale resolution based on the in-plane image magnification by surface plasmon polaritons *Phys. Rev. Lett.* **94**

[182] Huang B, Wang W, Bates M and Zhuang X 2008 Three-dimensional super-resolution imaging by stochastic optical reconstruction microscopy *Science* **319** 810–3

[183] Huang B, Babcock H and Zhuang X 2010 Breaking the diffraction barrier: Super-resolution imaging of cells *Cell* **143** 1047–58

[184] Rittweger E, Han K Y, Irvine S E, Eggeling C and Hell S W 2009 STED microscopy reveals crystal colour centres with nanometric resolution *Nat. Photonics* **3** 144–7

[185] Gao P, Prunsche B, Zhou L, Nienhaus K and Nienhaus G U 2017 Background suppression in fluorescence nanoscopy with stimulated emission double depletion *Nat. Photonics* **11** 163–9

[186] Zhao J, Jin D, Schartner E P, Lu Y, Liu Y, Zvyagin A V., Zhang L, Dawes J M, Xi P, Piper J A, Goldys E M and Monro T M 2013 Single-nanocrystal sensitivity achieved by enhanced upconversion luminescence *Nat. Nanotechnol.* **8** 729–34

[187] Gargas D J, Chan E M, Ostrowski A D, Aloni S, Altoe M V P, Barnard E S, Sanii B, Urban J J, Milliron D J, Cohen B E and Schuck P J 2014 Engineering bright sub-10-nm upconverting nanocrystals for single-molecule imaging *Nat. Nanotechnol.* **9** 300–5

[188] Mahalingam V, Mangiarini F, Vetrone F, Venkatramu V, Bettinelli M, Speghini A and Capobianco J A 2008 Bright white upconversion emission from $Tm^{3+}/Yb^{3+}/Er^{3+}$-doped $Lu_3Ga_5O_{12}$ nanocrystals *J. Phys. Chem. C* **112** 17745–9

[189] Wang F and Liu X 2009 Recent advances in the chemistry of lanthanide-doped upconversion nanocrystals *Chem. Soc. Rev.* **38** 976–89

[190] Debasu M L, Ananias D, Pastoriza-Santos I, Liz-Marzán L M, Rocha J and Carlos L D 2013 All-in-one optical heater-thermometer nanoplatform operative from 300 to 2000 K based on Er^{3+} emission and blackbody radiation *Adv. Mater.* **25** 4868–74

[191] Ye R, Xu C, Wang X, Cui J and Zhou Z 2016 Room-temperature near-infrared up-conversion lasing in single-crystal Er-Y chloride silicate nanowires *Sci. Rep.* **6** 34407

[192] Wu S, Han G, Milliron D J, Aloni S, Altoe V, Talapin D V., Cohen B E and Schuck P J 2009 Non-blinking and photostable upconverted luminescence from single lanthanide-doped nanocrystals *Proc. Natl. Acad. Sci.* **106** 10917–21

[193] Chen S, Weitemier A Z, Zeng X, He L, Wang X, Tao Y, Huang A J Y, Hashimotodani Y, Kano M, Iwasaki H, Parajuli L K, Okabe S, Loong Teh D B, All A H, Tsutsui-Kimura I, Tanaka K F, Liu X and McHugh T J 2018 Near-infrared deep brain stimulation *via* upconversion nanoparticle–mediated optogenetics *Science* **359** 679–84

[194] Wu X, Zhang Y, Takle K, Bilsel O, Li Z, Lee H, Zhang Z, Li D, Fan W, Duan C, Chan E M, Lois C, Xiang Y and Han G 2016 Dye-sensitized core/active shell upconversion nanoparticles for optogenetics and bioimaging applications *ACS Nano* **10** 1060–6

[195] Lucky S S, Soo K C and Zhang Y 2015 Nanoparticles in photodynamic therapy *Chem. Rev.* **115** 1990–2042

[196] Cheng L, Wang C and Liu Z 2014 Functional nanomaterials for phototherapies of cancer *Chinese J. Clin. Oncol.* **41** 18–26

[197] Frangioni J V. 2003 In vivo near-infrared fluorescence imaging *Curr. Opin. Chem. Biol.* **7** 626–34

[198] Williams S C P and Deisseroth K 2013 Optogenetics *Proc. Natl. Acad. Sci.* **110** 16287–16287

[199] Deisseroth K 2011 Optogenetics *Nat. Methods* **8** 26–9

[200] Zhang F, Vierock J, Yizhar O, Fenno L E, Tsunoda S, Kianianmomeni A, Prigge M, Berndt A, Cushman J, Polle J, Magnuson J, Hegemann P and Deisseroth K 2011 The microbial opsin family of optogenetic tools *Cell* **147** 1446–57

[201] Packer A M, Roska B and Häuser M 2013 Targeting neurons and photons for optogenetics *Nat. Neurosci.* **16** 805–15

[202] Nagel G, Szellas T, Huhn W, Kateriya S, Adeishvili N, Berthold P, Ollig D, Hegemann P and Bamberg E 2003 Channelrhodopsin-2, a directly light-gated cation-selective membrane channel *Proc. Natl. Acad. Sci.* **100** 13940–5

[203] Haase M and Schäfer H 2011 Upconverting nanoparticles *Angew. Chem. Int. Ed.* **50** 5808–29

[204] Liu B, Li C, Yang P, Hou Z and Lin J 2017 808-nm-light-excited lanthanide-doped nanoparticles: Rational design, luminescence control and theranostic applications *Adv. Mater.* **29** 1605434

[205] Wang C, Tao H, Cheng L and Liu Z 2011 Near-infrared light induced in vivo photodynamic therapy of cancer based on upconversion nanoparticles *Biomaterials* **32** 6145–54

[206] Cui S, Yin D, Chen Y, Di Y, Chen H, Ma Y, Achilefu S and Gu Y 2013 In vivo targeted deep-tissue photodynamic therapy based on near-infrared light triggered upconversion nanoconstruct *ACS Nano* **7** 676–88

[207] Idris N M, Gnanasammandhan M K, Zhang J, Ho P C, Mahendran R and Zhang Y 2012 In vivo photodynamic therapy using upconversion nanoparticles as remote-controlled nanotransducers *Nat. Med.* **18** 1580–5

[208] Lucky S S, Muhammad Idris N, Li Z, Huang K, Soo K C and Zhang Y 2015 Titania coated upconversion nanoparticles for near-infrared light triggered photodynamic therapy *ACS Nano* **9** 191–205

[209] Dong B, Xu S, Sun J, Bi S, Li D, Bai X, Wang Y, Wang L and Song H 2011 Multifunctional $NaYF_4:Yb^{3+},Er^{3+}$@Ag

core/shell nanocomposites: integration of upconversion imaging and photothermal therapy *J. Mater. Chem.* **21** 6193-6200

[210] Cheng L, Yang K, Li Y, Zeng X, Shao M, Lee S T and Liu Z 2012 Multifunctional nanoparticles for upconversion luminescence/MR multimodal imaging and magnetically targeted photothermal therapy *Biomaterials* **33** 2215–22

[211] Shan G, Weissleder R and Hilderbrand S A 2013 Upconverting organic dye doped core-shell nano-composites for dual-modality NIR imaging and photo-thermal therapy *Theranostics* **3** 267–74

[212] Meacham C E and Morrison S J 2013 Tumour heterogeneity and cancer cell plasticity *Nature* **501** 328–37

[213] Tian G, Zhang X, Gu Z and Zhao Y 2015 Recent advances in upconversion nanoparticles-based multifunctional nanocomposites for combined cancer therapy *Adv. Mater.* **27** 7692–712

[214] Wang Y, Wang H, Liu D, Song S, Wang X and Zhang H 2013 Graphene oxide covalently grafted upconversion nanoparticles for combined NIR mediated imaging and photothermal/photodynamic cancer therapy *Biomaterials* **34** 7715–24

[215] Xiao Q, Zheng X, Bu W, Ge W, Zhang S, Chen F, Xing H, Ren Q, Fan W, Zhao K, Hua Y and Shi J 2013 A core/satellite multifunctional nanotheranostic for in vivo imaging and tumor eradication by radiation/photothermal synergistic therapy *J. Am. Chem. Soc.* **135** 13041–8

[216] Fischer S, Bronstein N D, Swabeck J K, Chan E M and Alivisatos A P 2016 Precise tuning of surface quenching for luminescence enhancement in core-shell lanthanide-doped nanocrystals *Nano Lett.* **16** 7241–7

[217] Johnson N J J, He S, Diao S, Chan E M, Dai H and Almutairi A 2017 Direct evidence for coupled surface and concentration quenching dynamics in lanthanide-doped nanocrystals *J. Am. Chem. Soc.* **139** 3275–82

[218] Zou W, Visser C, Maduro J A, Pshenichnikov M S and Hummelen J C 2012 Broadband dye-sensitized upconversion of near-infrared light *Nat. Photonics* **6,** 560-564

[219] Wilhelm S 2017 Perspectives for upconverting nanoparticles *ACS Nano* **11** 10644–53